J. Phys. D: Appl. Phys. **30** (1997) 293–323. Printed in the UK PII: S0022-3727(97)56075-X

REVIEW ARTICLE

SQUIDs for nondestructive evaluation

W G Jenks†, S S H Sadeghi‡ and J P Wikswo Jr†

† Department of Physics and Astronomy, Vanderbilt University, Box 1807, Station B, Nashville, TN 37235, USA
‡ Amir Kabir University of Technology, Electrical Engineering Department, Hafez Ave, No 424, Tehran, Iran

Received 23 February 1996

Abstract. We attempt a comprehensive review of all published research in nondestructive evaluation (NDE) performed with the superconducting quantum interference device (SQUID) magnetometer since the first work was reported in the mid-1980s. The SQUID is the most sensitive detector of magnetic flux known. The energy sensitivity of the SQUID may make it the most sensitive detector of any kind. The research on SQUIDs for NDE is based on the promise of that sensitivity and on the various other desirable properties developed for SQUID instrumentation in biomagnetism and other fields. The sensitivity of SQUID instruments down to very low frequencies allows them to function as eddy-current sensors with unparalleled depth resolution, and to image the static magnetization of paramagnetic materials and the flow of near-dc corrosion currents. The wide dynamic range of the SQUID makes it possible to image defects in steel structures and to measure the magnetomechanical behaviour of ferromagnetic materials with high sensitivity. In the last decade SQUID instrumentation designed specifically for NDE has appeared and improved the spatial resolution of most work to roughly 1 mm, with promise of another order of magnitude improvement within the next five years. Algorithms for flaw detection and image deconvolution have begun to flourish. With many talented, industrious people in the field, the future of SQUID NDE looks bright, provided the crucial first niche can be found.

Contents

1. Introduction

The use of SQUIDs (superconducting quantum interference devices) has expanded tremendously since they became commercially available 25 years ago. The SQUID is an extremely sensitive magnetic flux-to-voltage transducer, and it is this extreme sensitivity that prompted its introduction into the field of electromagnetic NDE (nondestructive evaluation) a little over ten years ago. It is our goal to provide a comprehensive review of the work done and the progress made since that introduction. This may be the last chance for one review article to cover the entire field of SQUID NDE. The time is rapidly approaching when the field will be too large and progress too rapid for one article to accomplish this goal. This article is written for two audiences. First, it should be useful to students and researchers entering or considering entry into the field, allowing them to see the field as a whole and understand the rationale behind and methods of current work. Second, the quality assurance engineer and the process control engineer should be able to gain (from a thorough reading) a quantitative understanding of what can be done with SQUID NDE.

Work on SQUID NDE is most often reported first at the Applied Superconductivity Conference (ASC), the Review of Progress in Quantitative Nondestructive Evaluation (QNDE), and the European Conference on Applied

Superconductivity (EUCAS). Extensive proceedings from these conferences are published. Peer-reviewed journals which publish SQUID NDE work include the *Journal of Nondestructive Evaluation*, *IEEE Transactions on Applied Superconductivity*, *IEEE Transactions on Magnetics*, *British Journal of Nondestructive Testing* and *Cryogenics*. The reader is referred to these sources for future developments in the field.

The advantages of the SQUID for NDE include high sensitivity ($\approx$10–100 fT Hz$^{-1/2}$), wide bandwidth (from dc to 10 kHz), broad dynamic range (>80 dB), and its intrinsically quantitative nature. The high sensitivity of the SQUID allows one to make engineering and design compromises to reduce cost, enhance signal strength of particular types of flaws and still remain orders of magnitude more sensitive than other means of magnetic anomaly detection. The ability of SQUIDs to function down to zero frequency allows them to sense much deeper flaws than traditional eddy-current sensors, to detect and monitor the flow of steady state corrosion currents, and to image the static magnetization of paramagnetic materials. The wide dynamic range enables the SQUID to maintain its high sensitivity in the presence of strong dc or noise fields. The quantitative nature of SQUID NDE is often overlooked but is a valuable asset. The ability to model the NDE system response to particular flaw types without solving complex diffusion equations helps in the design of future instruments and will allow a rigorous probability of detection analysis for a conventional SQUID NDE system.

The scope of this paper is limited to SQUIDs applied to nondestructive evaluation near or above room temperature. SQUID imaging microscopes applied to samples in a cryogenic environment and remote sensing applications are discussed in brief. Early reviews of the field written by two of the pioneers of SQUID NDE, Weinstock [1] and Donaldson [2], are recommended to the reader. Wikswo [3] has provided a market-oriented overview of SQUIDs for biomagnetism and NDE. Cochran *et al* discuss design considerations for NDE instruments [4]. For a broader view of SQUID physics and applications the reader is referred to the many excellent articles by Clarke [5], and the book by Barone and Paternò [6].

In the context of NDE, one may summarize experimental SQUID magnetometry efforts in the past decade in three areas—flaw characterization, analysis of magnetic properties of materials, and corrosion study. In all of these areas, an extremely sensitive measurement of magnetic flux is made by the SQUID in order to give a picture of the magnetic field distribution in the vicinity of a test object. Magnetic field sources can be intrinsic in the test object, as in the case of galvanic currents flowing in a corroded specimen, or one may use an external source of energy to excite the test object for a resultant magnetic field. The external field excitation can be done either magnetically or electrically. With magnetic excitation, the test object is placed in a relatively strong magnetic field, whereas an ac or dc current is established in the sample for electrical excitation using the current injection or current induction method. In the injection method, the metal is directly connected to a current source, and for the case of current induction, eddy currents are generated within the inspected region by a coil or plate carrying an ac current.

As with other NDE techniques, recent theoretical and computational efforts in SQUID magnetometry have been directed toward devising imaging schemes that provide detailed information about the state of integrity of the material. These schemes are in general complicated and usually involve an inversion procedure in which the measured magnetic field is to be related to corresponding physical changes in the material.

Another aspect of SQUID magnetometry for NDE practices in recent years has been the development of new systems with arrays of smaller pick-up coils with smaller coil–sample spacings for improved imaging resolution. Furthermore, with the advent of high-temperature superconductors and low-cost refrigerators, new SQUID systems are being developed to be used conveniently for on-site applications.

The outline of this review paper is as follows. First, we give a brief overview of SQUID instrumentation basics. Then we review work on the study of magnetic field disturbances caused by flaws or change of magnetic properties of ferromagnetic materials. Flaw characterization, current localization, and corrosion in nonferrous metallic structures are then discussed. The application of SQUIDs to the nondestructive evaluation of nonmetallic materials is also reviewed. The present state of SQUID technology and its future trend in NDE practices is perhaps the most important part of this review as it pertains to the future of SQUID NDE. This is followed by developments in the problem of inversion and techniques for improved image processing. The advent of high-T_c SQUID systems has already been noted in the SQUID NDE community, and the time has passed when these systems should be discussed separately. The work with and the development of high-T_c systems is integrated throughout the text.

2. SQUID technology—an overview

This section provides a brief overview of SQUIDs. It is intended as a short tutorial for the novice user. The principles of operation, the methods of manufacture and the peripheral technology of SQUIDs are each discussed in turn.

2.1. SQUID operation

2.1.1. Superconductivity. For the reader unfamiliar with superconductivity, we briefly discuss those properties of superconductors necessary to understand SQUID operation. When cooled below a certain critical temperature, T_c, superconductors conduct dc currents with zero resistance. The maximum current the superconductor can carry with zero resistance is called the critical current, I_c. Superconductors also have unique magnetic properties. A superconducting ring will enclose only certain amounts of magnetic flux which are integer units of the flux quantum $\Phi_0 = 2.07 \times 10^{-15}$ Wb. The flux threading the ring is held

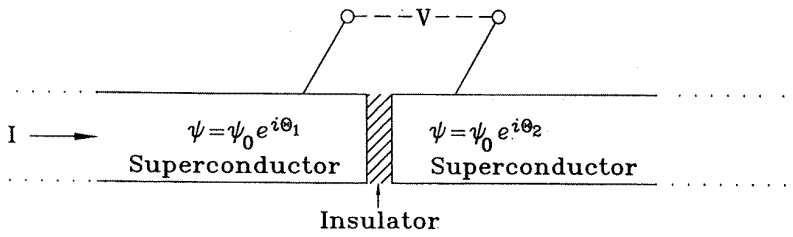

Josephson Equations

$$I = I_0 \sin\delta \quad \text{(dc)}$$

$$V = \frac{\hbar}{2e}\left(\frac{d\delta}{dt}\right) \quad \text{(ac)}$$

$$\delta = \Theta_1 - \Theta_2$$

Figure 1. The Josephson junction and Josephson equations. A superconductor is interrupted by a thin insulating layer (shaded area). The phase of the superconducting order parameter ψ becomes a function of the current flow through the junction, which leads to the unique electrical properties of the junction.

constant by superconducting currents which flow in the ring to oppose any change in flux applied to the ring.

The dominant superconducting materials used in SQUID fabrication today are Niobium and $YBa_2Cu_3O_{7-x}$. Niobium is a low-T_c metallic superconductor with T_c = 9.25 K. Typically, niobium SQUIDs are cooled by immersion in liquid helium, which has a boiling point of 4.2 K. $YBa_2Cu_3O_{7-x}$ belongs to a class of high-T_c superconductors which are conducting ceramics. It has a T_c of 93 K and can be operated in liquid nitrogen, which has a boiling point of 77 K. Liquid nitrogen is cheaper, easier to handle and has a far greater cooling power than liquid helium. At the present time, low-T_c systems dominate the research laboratories. For SQUID applications that do not require the absolute minimum SQUID noise, nitrogen-cooled high-T_c systems have a distinct advantage.

2.1.2. The Josephson junction. The Josephson junction [7] is the heart of SQUID technology. Figure 1 shows a typical junction and the Josephson equations which govern its electrical properties. While several physical configurations are possible, the essential feature of the junction is a thin insulating layer, or a narrow constriction, between two superconductors. The Josephson equations show that in two weakly connected superconductors, the relative phase $\delta = \theta_1 - \theta_2$ affects the electrical properties of the junction. The dc Josephson equation relates the applied current passing through the junction to the relative phase and the critical current of the junction I_0. The ac Josephson equation relates the voltage across the junction (once I exceeds I_0) to the temporal derivative of δ.

A SQUID is a superconducting loop containing two Josephson junctions (dc SQUID, figure 2(a)), or just one (rf SQUID, figure 2(b)). The SQUID is a weakly connected superconducting loop. A superconducting loop will contain flux only in multiples of the flux quantum, i.e. $n\Phi_0$, where n is any integer. Thus a change in the flux applied to the loop, Φ_A, will cause currents to flow to oppose that change and cause a phase difference across the junction. Typically, the SQUID incorporates a resistor in parallel with the Josephson junction(s) to prevent hysteresis in the I–V characteristic. The equivalent circuit of the ideal, noise-free, resistively shunted junction (RSJ) consists of the Josephson junction, its physical capacitance and the resistor, all joined in parallel, as shown in figure 2.

2.1.3. The dc SQUID. In the dc SQUID, a change in applied flux, Φ_A, leads to a phase difference across the junctions, giving rise to a voltage across the loop which we may detect. The characteristic I–V curves of the dc SQUID are shown in figure 3(a) for $\Phi_A = n\Phi_0$ and $\Phi_A = (n + 1/2)\Phi_0$, where n is any integer. If the bias current is held constant, the SQUID voltage will vary between two values, V_{min} and V_{max}, as the flux applied to the SQUID varies between $n\Phi_0$ and $(n + 1/2)\Phi_0$. The V–Φ_A curve is thus roughly sinusoidal, as shown in figure 3(b), with period Φ_0. Figure 3(c) shows that a small flux modulation, $\Phi_m \sin(\omega t)$ where $\Phi_m \leq \Phi_0/2$, applied to the SQUID operating at three different points, A, B, and C, on the V–Φ_A curve will elicit three different voltage responses V_s. At points A and C, V_s is at the same frequency as Φ_m, while at point B, where $\Phi_A = (n/2)\Phi_0$, V_s is at a frequency of 2ω. Thus the SQUID acts as a nonlinear flux-to-voltage transducer.

To linearize the V–Φ_A curve, we introduce the flux-locked loop (FLL) in figure 4. The FLL maintains lock by keeping the system at $\Phi = (n/2)\Phi_0$, one of the extrema in the V–Φ curve. A modulating flux, $\Phi_m(\omega)$ where $\Phi_m \leq \Phi_0/2$, is applied to the SQUID, at frequency ω, by the oscillator. The response of the SQUID is fed into a lock-in amplifier, referenced to the oscillator. If the dc flux in the SQUID is a multiple of $(n/2)\Phi_0$, then the output

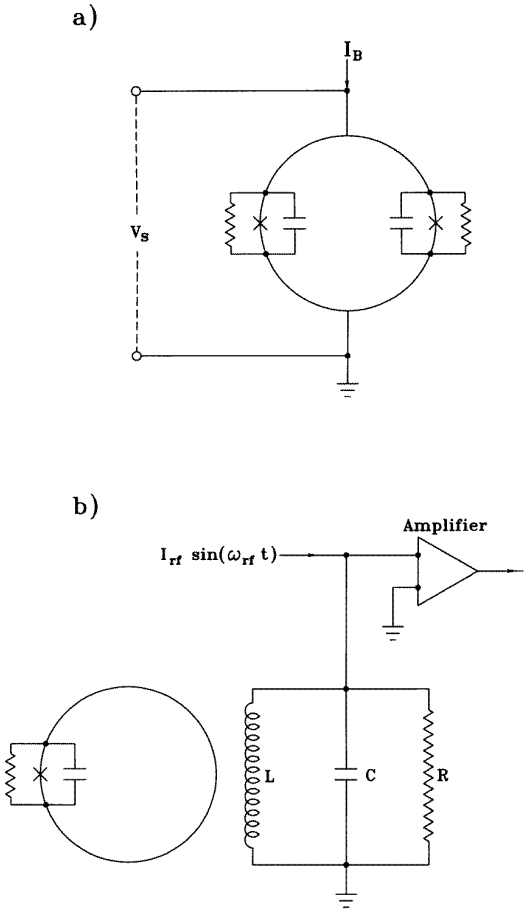

Figure 2. (a) Schematic of a dc SQUID loop. The superconducting loop is interrupted by two Josephson junctions, marked by $\times$. The dc SQUID is biased with a dc current. (b) Schematic of a rf SQUID loop. The rf SQUID has one Josephson junction, and the loop is inductively coupled to a rf tank circuit. The Josephson junctions are each shunted by a resistor. The physical capacitance of the junction is shown as well, because it must be considered in an accurate model of the electrical properties of the SQUID.

of the SQUID is a periodic function of 2ω and the lock-in amplifier will output 0 V dc. If the dc flux strays from an extremum by $\Delta\Phi$, then the SQUID output will contain a component at ω and the lock-in will output a dc voltage V_L proportional to the amplitude of the signal at ω, as shown in the lowest trace of figure 3(c). This dc signal is essentially an error signal; it is integrated and fed back into the modulation coil as $-\Delta\Phi$, returning the SQUID flux to $(n/2)\Phi_0$. The output of the loop V_0 is a voltage proportional to the feedback current, controlled by V_L (which is proportional to $\Delta\Phi$). The user records V_0 and relates that to the magnetic field through a prior calibration with a known field. The reader should note that many FLL oscillators output a square wave flux modulation with amplitude $\Phi_0/4$ and frequency ω. The system then shifts between $\Phi = (n/2+1/4)\Phi_0$ and $\Phi = (n/2-1/4)\Phi_0$, still centred on an extremum but spending very little time at the extremum.

The flux-locked SQUID has a bandwidth that is some fraction of the modulation frequency, typically 100 kHz

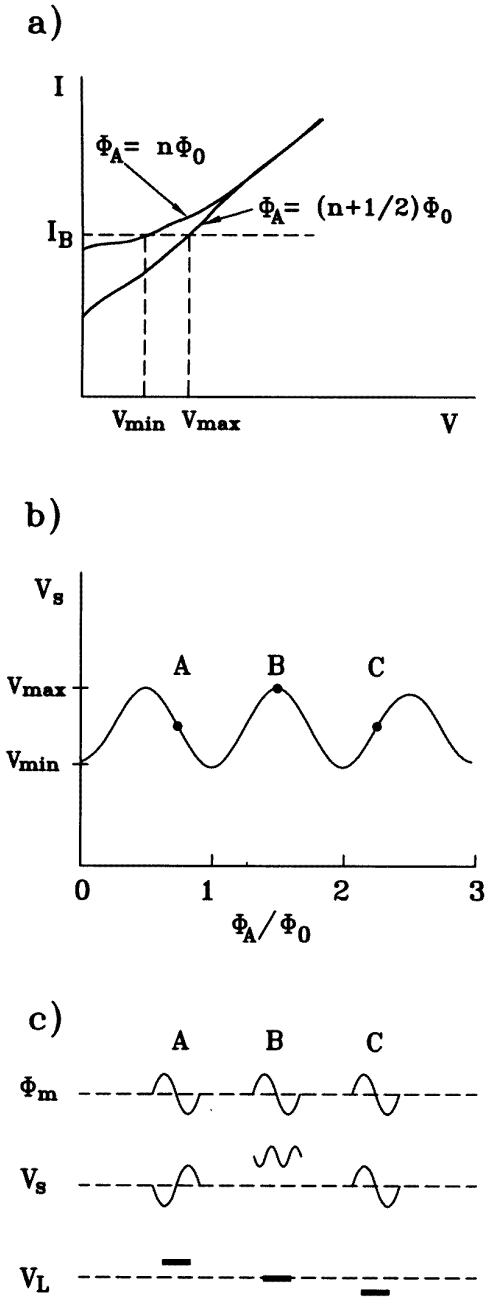

Figure 3. (a) The I–V characteristics of a dc SQUID. The amount of applied flux Φ_A determines the voltage output V_s for a particular value of bias current I_B. As the applied flux varies between $\Phi_A = n\Phi_0$ and $\Phi_A = (n+1/2)\Phi_0$, the output voltage changes between V_{min} and V_{max} (adapted from [5]). (b) The V–Φ curve of a dc SQUID, with constant bias current. (c) The voltage response of the SQUID to a modulating flux Φ_m. The response varies greatly depending on the value of Φ_A. Three possible points are highlighted to illustrate the response of a SQUID and the feedback needed to 'lock' the SQUID to operation at an extreme value. From top to bottom we see: one cycle of the flux modulation Φ_m applied to the SQUID operating at three different locations on the V–Φ curve; the voltage response of the SQUID V_s; and the necessary feedback of the flux-locked loop V_L which applies a counter flux to the SQUID loop to return the system to an extreme position on the V–Φ_A curve.

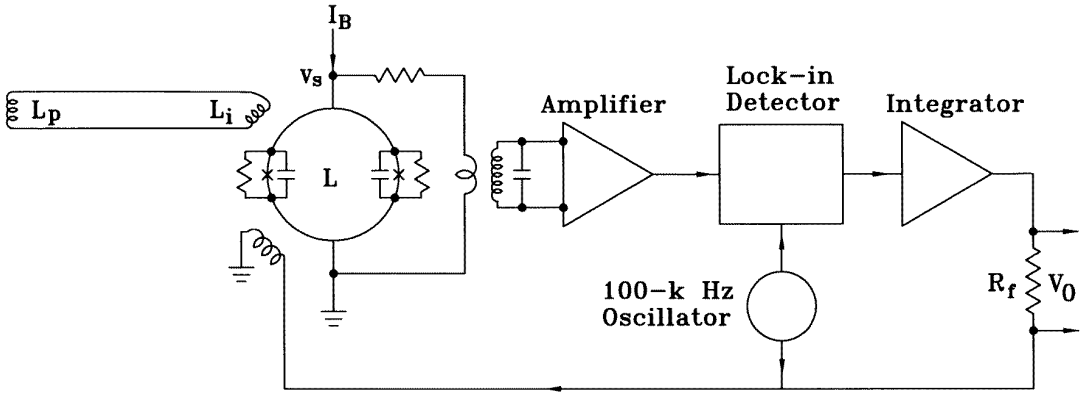

Figure 4. Schematic of the pick-up coil, input coil, SQUID and flux-locked loop (adapted from [5]). A change in magnetic field at the pick-up coil, with inductance L_p, induces a change in field at the input coil, with inductance L_i. The SQUID is inductively coupled to the input coil and detects a change in magnetic flux. The voltage response of the SQUID V_s is the input to the flux-locked loop, which uses a modulating flux scheme, explained in the text, to maintain the SQUID at an extremum on the V–Φ curve. The user measures a change in V_0, which is proportional to the feedback from the loop and hence to the change in magnetic field at the pick-up coil.

modulation and 10 kHz bandwidth, although operation at higher frequencies is common. If the applied flux changes too rapidly for the feedback electronics to track, then the SQUID jumps from one extremum to another, and the SQUID is said to have lost lock. The maximum change in flux per unit time that the system can tolerate while maintaining lock is the slew rate, typically $\approx 10^6 \Phi_0$ s^{-1}. The majority of SQUIDs used for NDE work to date are low-T_c, dc SQUIDs, which have the best sensitivity and are the standard in the biomagnetic community.

2.1.4. The rf SQUID. Conceptually, the operation of the rf SQUID is very similar to its dc counterpart. The rf SQUID is inductively coupled to a tank circuit, as shown in figure 2(b), being driven at a typical frequency $f_{rf} \approx 20$–30 MHz. If the magnitude of the rf current in the tank circuit I_{rf} is kept constant, then the voltage across the circuit V_{rf} will be periodic with any flux applied to the SQUID. This holds true because of the hysteretic nature of flux in the SQUID loop. The V_{rf}–Φ curve is then linearized with a flux-locked loop in a manner similar to the dc SQUID. In this case, the modulating flux is applied through the inductor in the tank circuit. High-T_c SQUIDs can be made either dc or rf, but so far rf SQUIDs are preferred in NDE work because of the difficulty in connecting directly to the SQUID loop.

2.1.5. The pick-up coil. The SQUID is an excellent sensor of magnetic flux. To enhance its capabilities, most SQUID systems do not expose the bare SQUID to the magnetic field of interest. Rather, they typically employ a multi-turn pick-up coil inductively linked to the SQUID as shown in figure 4. The pick-up coil, with inductance L_p, senses the ambient field while the input coil, with inductance L_i, and the SQUID, with inductance L, are shielded from the ambient field by a superconducting niobium canister. Typical values for the inductances are $L_p = L_i = 1$ μH and $L = 0.1$ nH. Historically, all pick-up coils were hand wound of superconducting wire, but in some thin-film configurations the pick-up coils are now fabricated on the same chip as the SQUID or on an adjacent 'flip chip' using integrated circuit technology. These are of particular utility with high-T_c SQUIDs.

2.1.6. Noise in the SQUID. SQUID noise is quoted in different units by different members of the SQUID community. The given noise figure is generally a power spectral density in terms of energy (J Hz^{-1}), magnetic flux (Φ_0 Hz$^{-1/2}$), field (fT Hz$^{-1/2}$) or field gradient (fT cm^{-1} Hz$^{-1/2}$). The distinction is important as one system (of special design) can have poor field sensitivity, despite superior energy sensitivity in the SQUIDs it contains. The energy and flux noise are figures of merit (FOM) for the bare SQUID, while the field and field gradient noise are FOM for the complete SQUID system. As a rule of thumb, the SQUID researcher quotes energy or flux noise, while the SQUID system builder begins with the flux figure and designs for the best possible field or field gradient noise, which is of paramount interest to the end user. Typical orders of magnitude for commercial dc SQUIDs are: noise energy $\epsilon = 10^{-31}$ J Hz^{-1}; magnetic flux noise $S_\Phi^{1/2} \sim 10^{-6}$ Φ_0 Hz$^{-1/2}$; and magnetic field noise $B_N = 10$ fT Hz$^{-1/2}$.

SQUID noise is not of grave concern in SQUID NDE because in any real application environmental noise is expected to dominate the signal. This is not particularly true for all high-T_c SQUIDs in use today, but we assert that with the current pace of progress it will be before any instrument is brought to market. Flicker or $1/f$ noise does exist in thin-film SQUIDs. Only below ~ 0.1 Hz does it begin to dominate in conventional niobium SQUIDs, and the best high-T_c SQUIDs have a $1/f$ knee around 1 Hz. Presently, some high-T_c SQUIDs exhibit additional noise if operated in an applied, dc magnetic field.

2.2. Design and manufacture of SQUIDs

2.2.1. Low-T_c SQUIDs. Modern thin-film SQUIDs are typically manufactured by sputtering of niobium thin films and patterning the films by photolithography or electron beam lithography. In principle any superconducting material can be used to manufacture SQUIDs, but in practice niobium technology completely dominates the low-T_c commercial SQUID market. The junction itself may be a $Nb/NbO_x/Pb$ or $Nb/Al_2O_3/Nb$ trilayer, while the resistive shunts can be a thin film of copper, gold, or nearly any metal which does not superconduct at 4 K.

2.2.2. High-T_c SQUIDs. Thin-film SQUIDs have been constructed from all the main families of high-T_c compounds: Y–Ba–Cu–O, Bi–Sr–Ca–Cu–O and Tl–Ba–Ca–Cu–O. The material that has come to dominance is $YBa_2Cu_3O_{7-x}$. Josephson junctions have been manufactured in a number of ways using this material. The two main types of junction are grain boundary and superconducting–normal–superconducting (SNS) junctions, i.e. $YBa_2Cu_3O_{7-x}$–N–$YBa_2Cu_3O_{7-x}$, junctions where N represents a normal metal such as gold or silver. With the current state of the technology, the best grain boundary SQUIDs have the lowest noise, but the best SNS junction SQUIDs are more rugged, reproducible and manufacturable. The main difficulties with early high-T_c SQUIDs were high $1/f$ noise and poor performance when operated in weak environmental magnetic fields such as the Earth's field. Due to improvements in manufacturing and advanced feedback schemes [8], $1/f$ noise is no longer an impediment to applying high-T_c SQUIDs to electromagnetic NDE, where 'very low frequency' means of the order of fifty Hertz. Operating in the Earth's field, good quality $YBa_2Cu_3O_{7-x}$ SQUIDs already have less noise and greater sensitivity than flux-gate magnetometers. The best high-T_c SQUIDs are getting better but the optimum high-T_c SQUID system has yet to be made.

2.3. SQUID systems

A generic low-T_c SQUID instrument [9] is depicted in figure 5. We see that the SQUIDs are located inside a small magnetic shield (e.g. superconducting niobium). Superconducting pick-up coils are located at the bottom of the Dewar, the SQUID electronics are at room temperature, but close to the Dewar, and the magnetic object is placed beneath the instrument. If the experiment is conducted in an applied magnetic field, then the instrument is a susceptometer. Extreme sensitivity to environmental fields is a serious problem in the development of high-T_c SQUID systems, primarily because high-T_c magnetic shields and wire do not perform as well as the equivalent niobium components. This is likely to be a problem for some time, since all known high-T_c compounds are extreme type II superconductors, which lose perfect diamagnetism at very low critical fields, H_{c1}. Some partial solutions to these problems have been developed and will be discussed in section 8.

The term SQUID is used very freely within the SQUID community. It may refer to the SQUID loop, the face of the pick-up coil, part or all of the superconducting components, or the entire instrument. The reader is expected to grasp the exact meaning from the context. We follow this convention, except where an ambiguity could deceive the reader.

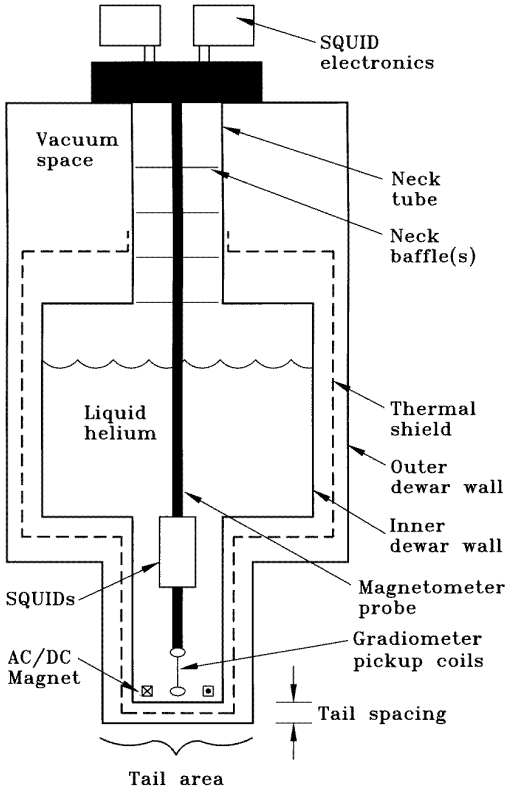

Figure 5. A cross sectional schematic of a simple low-T_c SQUID gradiometer system. The SQUID and input coil, housed in a superconducting niobium cylinder, are inductively coupled to an axial gradiometer near the tail of the Dewar. The flux-locked loop is within the SQUID electronics box above the Dewar and linked to the SQUID through the magnetometer probe. The Dewar is filled with liquid helium (boiling point 4.2 K) to cool the superconducting SQUID, niobium shield and pick-up coils. The Dewar is insulated by a vacuum space between the inner and outer walls. The instrument may be used to sense the intrinsic magnetic field of a sample or, with the magnet energized, it can measure the response of the sample to an ac or dc magnetic field (adapted from [9]).

2.3.1. Noise and environmental field rejection. Although a simple single or multiple loop pick-up coil (a magnetometer coil) can be used to measure one component of the magnetic field, such as B_z, there are a number of disadvantages to this approach, the most important of which are the contamination of the signal by environmental noise and extreme sensitivity to tilt in the magnetic field of the Earth. Since the field of interest is generally orders of magnitude smaller than power line noise, fields from passing vehicles and radio frequency interference, some means of background field rejection is required. This can be done by shielding the entire experiment, which is difficult and expensive in most NDE applications. Gradiometry is generally preferred. Gradiometers [10] take advantage of

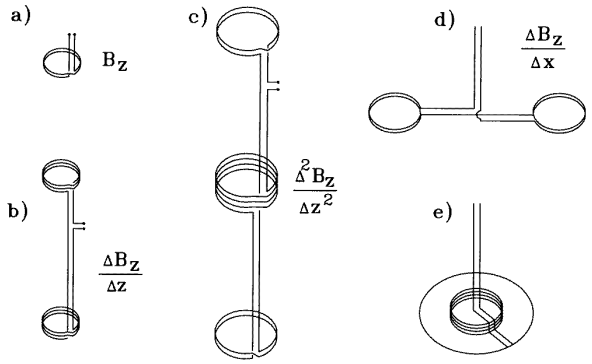

Figure 6. A variety of pick-up coil designs and the physical quantity they measure: (a) magnetometer; (b) first-order axial gradiometer; (c) second-order axial gradiometer; (d) first-order planar gradiometer; and (e) first-order radial gradiometer.

the mathematical form of the fall-off of magnetic fields with distance from the source. The local source of interest generates a much larger field gradient at the detector than does the more distant noise source, even though the absolute noise field is larger and the magnetic field may be of more interest than the gradient. Thus, by configuring coils to sense the magnetic field at two or more locations, it is possible to discriminate against the distant sources and in favour of the local one. In low-T_c technology, the input coil is connected in series with two or more pick-up coils, which are outside the SQUID's niobium shield. For example, we may sense $B_z(z_1)$ with one loop of the gradiometer coil, $B_z(z_2)$ with a second loop wound in the opposite sense, and the SQUID reports a voltage proportional to $\Delta B_z/\Delta z$, where $\Delta z = z_2 - z_1$. Some typical designs for wire-wound gradiometers are shown in figure 6.

Electronic synthetic gradiometer systems, which incorporate multiple SQUIDs, have been developed to allow high-T_c systems to function in noisy environments [11, 12]. These function by placing the SQUIDs in the locations of the sensing loops in low-T_c systems and electronically subtracting the outputs. Here we may sense $B_z(z_1)$ with one SQUID, $B_z(z_2)$ with a second SQUID, and the SQUID electronics report a voltage proportional to $\Delta B_z/\Delta z$.

Most SQUID systems used for NDE research are gradiometric. However it is typical to report the SQUID output in units of magnetic field. This is because with many axial gradiometers the derivative approximates B_z due to the proximity of the sample and the uniformity of the noise fields. The reader is cautioned that this convention is sometimes followed with little justification.

2.3.2. Cryogenic Dewar design. Liquid helium is required to maintain conventional (low-T_c) SQUIDs and coils in the superconducting state. The superconducting components are generally immersed in a helium reservoir which is thermally insulated with a vacuum jacket containing carefully designed radiation shields. Dewars are constructed with fibreglass-reinforced epoxy, which has been found to have suitable structural and thermal properties without introducing Johnson noise, distorting uniform noise fields, or screening the magnetometer from low-frequency signals. Most magnetometer measurements can be improved by minimizing the separation between the pick-up coils and the room-temperature environment, and this has led to Dewars in which the superconducting components are in the vacuum space, thermally coupled to the helium [13].

Dewar design is critical to SQUID NDE. SQUID NDE systems are designed to measure the magnetic field very close to the surface of the samples under inspection. The resolution of the images is roughly determined by the greater of the size of the pick-up coil and its distance from the magnetic source. The early SQUID NDE work we will discuss was generally performed with SQUID systems with a spatial resolution of 1 cm or higher; the modern SQUID NDE system has a resolution of roughly 1 mm.

3. SQUID NDE of ferromagnetic materials

Conventional magnetic methods of NDE have been in use for more than forty years. In these techniques, the specimen is usually magnetized, and the presence of a surface or subsurface flaw is detected by monitoring the magnetic flux leakage outside the metal using a field-sensitive indicator such as a Hall effect probe, magnetoresistive sensor or inductive pick-up coil, or by using magnetic inks and powder. The advent of SQUIDs as highly sensitive magnetic flux detectors has enabled measurement of small spatial variations of a weak magnetic field. For example, it is not necessary to apply a very large magnetizing field (say 700 A m^{-1}) to the specimen in order to produce a detectable flux leakage, as is the case with conventional approaches. Also, it is possible to place the sensing probe at a relatively larger distance from the specimen. In addition to this type of conventional magnetic anomaly detection, SQUIDs are used to monitor the very weak magnetization signature due to the mechanical state of a ferromagnetic material. This use of SQUIDs may lead to the prediction (as opposed to the detection) of fatigue damage in steel components and structures.

3.1. Flaw detection and characterization

Gordon Donaldson and his group at the University of Strathclyde, Scotland, utilized SQUIDs for the detection of flaws in steel plates [14–17]. In their early system, they used a planar gradiometer connected to a RF SQUID and a superconducting solenoid applied static magnetic field perpendicular to the test plate, as shown in figure 7(a). A radial planar gradiometer was used to eliminate sensitivity to the axial gradient of the field that is the result of inevitable variations in the field–specimen separation during the scanning process. This system is similar in design to a biomagnetic susceptometer previously developed by Wikswo and co-workers at Stanford [18]. Experiments on steel plates showed that machined slots with cross sections as small as 2×1 mm^2 could be detected at a lift-off distance of 4.2 cm. Figure 7(b) shows typical results associated with scanning 20, 40, and 80 mm long slots of 6×6 mm^2 cross

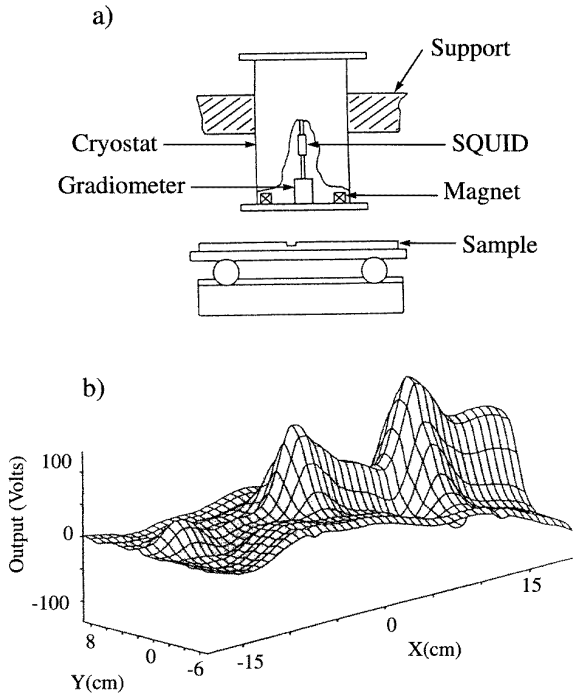

Figure 7. (a) Schematic of an early SQUID scanning system used to detect slots cut in a steel plate. The rf SQUID is coupled to a planar gradiometer at the bottom of the cryostat. A superconducting magnet imposes a static magnetic field on the steel plate. The plate is scanned in the x–y plane 5 cm below the magnetometer. (b) The SQUID output recorded as the plate is scanned. It was demonstrated that the SQUID could locate and roughly size the slots. (From [14] and [16], with permission.)

section at 5 cm lift-off. It was also shown that the detection capability is not governed by the SQUID noise limit, rather by the variation in residual magnetic fields in the specimen, for example due to spatial fluctuations of the permeability in the vicinity of flaw. To improve the detection resolution, the cryostat tail was modified [19] to reduce the minimum lift-off from 20 mm to 2 mm and the inner coil diameter from 20 mm to 2 mm. The Strathclyde group then began a study [4] of more realistic steel samples which included a 30×30 cm^2 piece of a 12.5 mm thick UK naval hull plate which had an artificially produced surface-breaking fatigue crack. By mapping the distortions in the applied static field above the plate, they were able to identify the position of the crack, its orientation and regions of greater crack growth.

Bruno *et al* [20], of the Catholic University in Rio de Janeiro, in collaboration with Wikswo's group at Vanderbilt University demonstrated the detection of 0.1 mm^3 surface-breaking flaws in a steel plate by using a SQUID desensitized to work near the surface of ferromagnetic materials. They showed that, at close range, the depth of a shallow flaw could be estimated by the SQUID response. It was also reported that with extreme low pass filtering the SQUID could detect flaws 1 cm below the surface.

The detection of cracks in the steel reinforcing rod (rebar) of concrete structures has been demonstrated [21] by Braginski's group at KFA in Jülich, Germany. In collaboration with workers from materials testing and construction materials research institutes, the KFA group used a high-T_c SQUID system to scan a prestressed steel element of an autobahn three-lane bridge. Using a system with normal state pick-up coils connected to a stationary SQUID they found that they could localize the supporting stirrups and identify a known rupture in the rebar. Their results showed that the greater linearity and dynamic range of the SQUID/normal gradiometer system made it superior to a conventional Hall probe magnetometer, even though the use of normal state pick-up coils with a SQUID reduced the sensitivity and the bandwidth of the instrument.

3.2. Magnetic properties of steels

It is well known that the presence of stress affects the magnetic state of a ferromagnetic material by rotating the magnetization of magnetic domains or moving the magnetic domain wall at microscopic levels. Studies of the changes in the magnetic state of the material might identify the source or distribution of stress.

Weinstock and Nisenoff [22, 23] were the first to demonstrate the applicability of SQUID magnetometry for the study of stress–strain behaviour in a ferromagnetic material. In their experiment, a second-order gradiometer was placed 20 cm away from a steel bar undergoing stress. They showed that the magnetic flux measured outside the bar changes as the strain is increased. The change in the magnetic flux was not monotonic even below the elastic limit of the material. In the plastic regime, the irreversibility of the stress–strain curve was similarly observed in the measurement of the magnetic flux. The study also showed that at roughly 60% of the elastic limit, the sign of the magnetoelastic coefficient changes. They proposed that this phase reversal phenomenon could be used to indicate the onset of fatigue in steel.

The capability of SQUID magnetometry for evaluation of stress-related deformations in ferromagnetic materials was examined further by Mignogna and Chaskelis [24]. They used both a conventional flux-gate magnetometer probe and a SQUID magnetometer to monitor the magnetic field variation of steel and nickel samples under cyclic loading. This work confirmed the phase reversal phenomenon in steel, although it was not observed in the case of nickel. The effect in steel was shown to be more complex, with multiple changes in the magnetoelastic coefficient. In a subsequent collaboration [25, 26], a rotating, nonferromagnetic load frame, in which samples could be stressed, was mounted onto an x–y translation stage beneath a three-axis SQUID gradiometer for the purpose of scanning ferromagnetic samples during cycling. This machine can map the x, y, and z components of the magnetic field over the surface of an entire specimen.

Recent work [27, 28] by Weinstock and collaborators at the INSA de Lyon in France investigated the magnetomechanical hysteresis curve of several steels. They have shown an increase in the area of the magnetomechanical hysteresis curve of samples of a standard French steel (designated E24-2) after repeated cycling to seven-tenths the elastic limit. Their apparatus

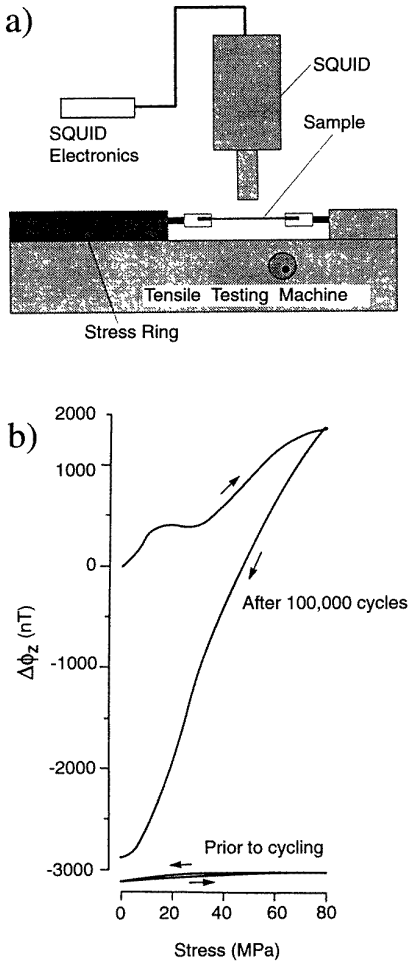

Figure 8. (a) SQUID system for the measurement of changes in the ambient field near a steel sample under stress cycling. (b) The output signal ($\Delta\phi$) as a function of applied stress (load) for an annealed E24-2 steel bar before and after 100 000 fatigue cycles to 168 MPa. (From [27], with permission.)

and the hysteresis curve before and after cycling are shown in figure 8. Note that the area of the curve for the fatigued specimen increased dramatically after repeated cycling. The growth in this area or lack thereof under cycling may indicate the presence or absence of fatigue.

The changes in the magnetic state of a ferromagnetic material may also be monitored by the analysis of Barkhausen emission. In this phenomenon, the transition between reversible to irreversible magnetization regions in some ferromagnetic materials occurs by producing small abrupt jumps in magnetization. The feasibility of using a SQUID for the analysis of Barkhausen emission was demonstrated by Weinstock and co-workers [29]. In that work, a biomagnetic gradiometer was used to detect the Barkhausen jumps in magnetization of a polycrystalline iron pill or wire which was placed in a slowly varying weak magnetic field. Barkhausen NDE with conventional detectors has progressed beyond the laboratory stage and SQUID detection of Barkhausen emission has a distinct advantage in its broad bandwidth and high sensitivity. SQUID detection of Barkhausen emission is well worth more extensive exploration.

In another application [30], Donaldson's group, in collaboration with a group from Hitachi, utilized a SQUID gradiometer to investigate the effects of aging at high temperatures in several samples of Duplex stainless steel. Aging is a change in a metal by which its structure recovers from an unstable condition produced by quenching or by cold working. The change in structure often consists of precipitation, often submicroscopic, and can be marked by an undesirable change in physical properties, such as embrittlement. In the case of Duplex stainless steel, precipitation may also cause the movement or rotation of magnetic domains, giving rise to variations in local magnetic properties. It was shown that the measurement of the remanent field by a SQUID during aging can monitor the aging process. Although other conventional techniques could be used for the study of the hysteresis measurements, the importance of this application is the use of a noncontacting scheme which performs measurements as far as 9 cm from the test object. This can be a great advantage if the object is hot.

The Hitachi group has done further work [31], utilizing a custom-built SQUID mounted on a computer-controlled robot arm for the scanning of stainless steel under stress. They showed that under controlled conditions, the SQUID could detect fatigue damage before fatigue crack initiation in a stainless steel (type 304) sample undergoing strain cycles in a dc magnetic field. Specifically, they measured a monotonic rise in maximum SQUID output with the number of cycles and showed that a knee in the output versus cycles curve occurs at a value of roughly $1/100$ of the expected number of cycles to failure.

Commercial SQUIDs have been used to measure the magnetic moment and magnetic properties of ferromagnetic thin films for many years. Recently SQUID systems have been developed for *in situ* measurements on Fe/Cr and Co/CoO thin films in the ultrahigh vacuum growth environment. Pappas *et al* [32] reported a sensitivity corresponding to the growth of an additional 0.1 atomic layer of iron. With their system they could briefly suspend growth and measure the magnetic moment, then proceed with the growth. In this way data corresponding to the growth of dozens of films of varied thickness could be collected in one experiment. Spagna *et al* [33] modified a sophisticated quantum design system and linked it to a molecular beam epitaxy (MBE) facility. Their SQUID measurements, e.g. magnetic hysteresis at $T = 50$ K and $H_{Applied} \leq 1$ T, could be performed within 2 min of growing their cobalt thin films without breaking the ultrahigh vacuum. With these systems excellent science characterizing the growth process of magnetic thin films can be carried out. Multi-SQUID systems of similar design could one day be used in the quality assurance of magnetic thin films.

4. SQUID NDE of nonferromagnetic conducting materials

Electromagnetic techniques have been utilized extensively for nondestructive evaluation of conducting structures

[34†]. In these techniques, the objective is to produce an electromagnetic field in the body under test and to measure the field perturbations caused by probable flaws in the metal, using an appropriate sensor. Eddy-current and potential difference techniques are the most commonly used methods in electromagnetic NDE practices.

In the eddy-current approach, an alternating current is used to induce eddy currents in the metal body under study. If the eddy currents are affected by the presence of a flaw, there will be a change in the impedance of the inducing coil. By measuring and analysing the variation of the coil impedance, it is possible to detect and size flaws in metals. In conventional eddy-current testing, the operating frequency typically ranges between 100 kHz–10 MHz. The signal (coil impedance) decreases and instrumental noise increases as the operating frequency is decreased. As a result, since the current skin depth in metal is inversely proportional to the square root of the operating frequency, it follows that the eddy-current approach is inherently incapable of detecting deep flaws in good conductors. When applied to deep flaws the eddy-current technique has limited spatial resolution because the sensing coil must be large enough to produce a measurable flaw signal in the presence of noise. It is common practice to use a pick-up coil with a few hundred turns and a diameter of several millimetres. Hence, the compromise is between spatial resolution and signal strength. In addition the inversion of the impedance data requires the solution of complex diffusion equations [35].

In the potential difference technique, an ac or dc current is established in the metal and the electrical potential difference between the two conducting legs of a contacting probe is used to detect the presence of a crack. The main problem associated with the potential drop technique is that the reliability of the flaw detection severely depends on establishing a good electrical contact between the probe and the metal under test. In fact, the loss of contact due to oxidization of the metal surface or the existence of nonconducting particles on uncleaned surfaces can result in an incorrect indication of cracks. Furthermore, the technique is essentially ineffective in the inspection of structures whose surfaces are covered by layers of insulating materials such as paint or anodization.

SQUID magnetometry can be an alternative to conventional electromagnetic techniques for NDE of metallic structures, because it provides an extremely sensitive, low-noise measurement of magnetic field in the range of dc to 10 kHz. This enables SQUID technology to overcome the practical limitations we have outlined for conventional eddy-current measurements. In addition to the traditional applications of flaw characterization and localization of conducting structures, the dc sensitivity of the SQUID allows it to be used to study the quasi-static currents of active corrosion in metals. It should be pointed out that while this section covers SQUID NDE of nonferrous metals, all the techniques discussed here can be applied to ferrous metals with some added complication from the hysteretic nature of the specimens. Donaldson's group has successfully demonstrated the application of these techniques [4] to one of their steel plate samples.

† This work is particularly recommended to the reader.

4.1. The current injection technique

Weinstock and Nisenoff [22] were the first to demonstrate the capability of SQUID magnetometry for the detection of flaws in conducting structures. In their experiment they used a second-order gradiometer and a 1 A, 4.6 Hz ac current injected into copper and iron pipes to show that the SQUID measurement of the magnetic field distribution around the pipe at a distance well above the pipe ($\approx$ 20 cm) can be used to detect the presence of various holes. Although no attempt was made to measure the size of the holes, the experiment clearly proved that SQUIDs could be utilized for monitoring small magnetic field perturbations due to the variation of current deflected by a flaw in conducting structures.

Following the work of Weinstock and Nisenoff, Wikswo and his group at Vanderbilt University began to apply SQUID magnetometry to the NDE of metallic structures. To conduct their NDE experiments, they utilized a high-resolution SQUID magnetometer [13], termed MicroSQUID, which had been developed for imaging biomagnetic sources with a resolution of 1 mm. This type of high-resolution magnetometer has come to dominate SQUID NDE and will be discussed in the subsequent section on SQUID NDE systems.

The early experiments with MicroSQUID involved the application of the technique proposed by Weinstock and Nisenoff to detect flaws in planar conductors [36, 37]. As shown in figure 9, a thin sheet with a small hole drilled through the centre was injected with a uniform current. The hole perturbed the current flow and caused an aberration in the normal component of the magnetic field B_z which was imaged by repeated scans of the sheet beneath the SQUID. The Vanderbilt group showed that circular holes as small as 350 μm in copper and aluminium sheets can be detected. (Note that the current level ($<$10 mA) is extremely low compared to other NDE techniques). The dipolar signal of the flaw in figure 9 may be understood by a simple law-of-superposition exercise. The magnetic field from the flawed current-carrying plate can be thought of as the field of an unflawed plate added to the field of a disc of current, the size of the flaw, flowing in the opposite direction. For a sufficiently large plate, the contribution of the plate to the normal field, B_z, is negligible while the disc of current has a predominantly dipolar field. Despite the capability of MicroSQUID to detect flaws in conducting plates, it was observed that the characterization of the signature of the flaw suffers from a substantial background signal, as shown in figure 9(b). The finite plate is only an approximation of an infinite plate; for an infinite sheet of current, B_z must be zero from symmetry arguments alone. Furthermore the field from the edges of the plate tends to dominate the image.

In order to investigate the problem systematically, a theoretical study of the field–flaw interaction for an infinite conducting sheet was carried out [38]. A comparison of the experimental results with their theoretical counterparts indicated that the problem could be traced to the finite size of the samples. In fact, the signals associated with the currents around plate edges as well as the lead-in wires were found to be several orders of magnitude larger than the flaw signal. To overcome this problem, a technique

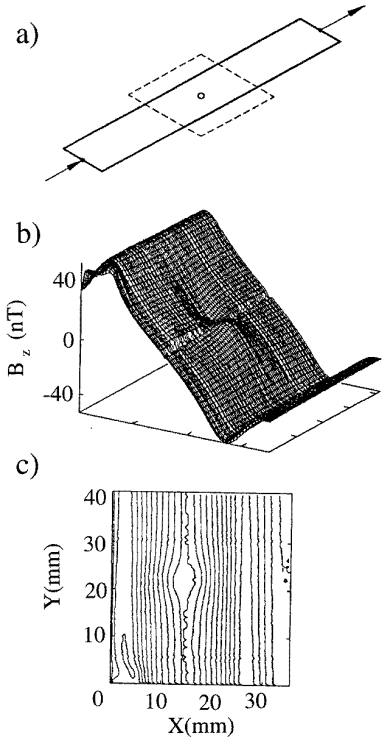

Figure 9. Magnetic field recording above a 32 μm thick copper sheet with a 3 mm hole in the centre. (a) The flawed copper sheet, measuring 25 mm $\times$ 150 mm $\times$ 32 μm carrying a 7.5 mA, 1.6 Hz current. The dotted square represents the region scanned with MicroSQUID. (b),(c) Surface and isofield contour plots of B_z measured in the x–y plane 2.8 mm above the copper sheet (5 nT contours) showing the perturbation due to the flaw superimposed on the large background slope. Note that the signature of the flaw is that of a current dipole with polarity opposite that of the sheet current. (From [39], with permission.)

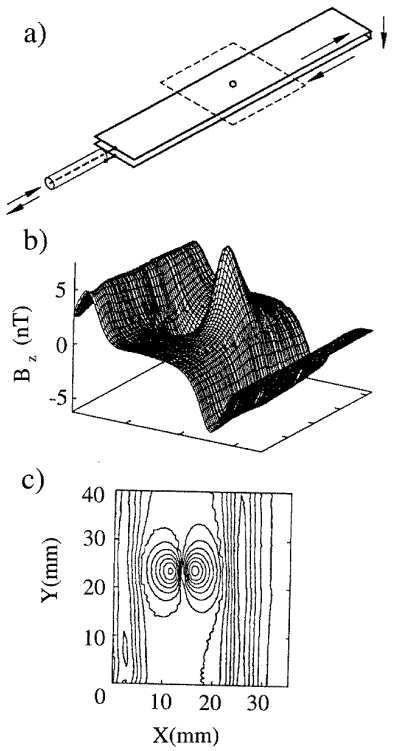

Figure 10. Cancellation plate technique applied to the current-carrying sheet with the 3 mm hole, shown in figure 9. (a) An unflawed return plate of the same dimensions as in figure 9 was placed 0.45 mm below the flawed sheet and the two were connected in series. (b), (c) Surface and isofield contour plots of B_z measured above the two plates (1 nT contours). The background slope was nearly cancelled and the flaw can be seen with much greater resolution. (From [39], with permission.)

was developed [39] which substantially eliminated the background signal. In this technique, shown in figure 10, an unflawed conducting sheet is placed beneath and parallel to the flawed plate. The plates are electrically connected in series at one end. At the opposite end, a coaxial cable is used to inject current into one plate and retrieve it from the other plate. With this arrangement it was shown that the magnetic field due to the edges of the sample plate are essentially cancelled and the interfering signal due to the current cables is remarkably reduced. The cancellation principle was also studied [39] for transverse and longitudinal currents flowing in tubes and rods and later applied [40] to such samples. One of the key elements in the research at Vanderbilt has been the development of theoretical modelling in parallel with experimental work. This has been crucial in understanding the field–flaw interaction while establishing inversion schemes which can predict the size of a flaw. For example, a finite element algorithm was developed to calculate the magnetic field outside a current-carrying metal sheet containing circular or elliptical flaws [41]. In the case of a circular hole in thin plates mentioned above, it was shown that in the far-field region, i.e. when the flaw is much smaller than the distance between the flaw and the SQUID, the peak-to-peak amplitude of the flaw signal is directly proportional to the area of the flaw and the separation between the peaks in the magnetic field is $\sqrt{2}$ times the depth of the flaw beneath the magnetometer measurement plane.

The problem of injected current in flawed metallic sheets has also been investigated at MIT [42]. Gans and Rose used a SQUID with second-order gradiometer pick-up coils to demonstrate the detection of holes as small as 750 μm. Subtracting the data from two SQUID channels they formed a software planar gradiometer which was able to reject the background signal associated with the edges of the plate.

The Vanderbilt group then extended their theoretical and experimental work to tackle the problem of flaws in three-dimensional conducting structures. In this connection, the problem of circular or elliptical holes in current-carrying conductors was first investigated [43]. An analytical solution was obtained which can determine the distribution of the magnetic field outside the conductor. This modelling is particularly useful for simulating cracks of very small opening by setting to zero the value of the minor axis of the ellipse. Based on the theoretical examination of the magnetic field distribution, an inversion technique was developed to determine the size, location

and orientation of the crack. The problem of cylindrical holes was extended to cylindrical flaws of finite depth [44]. The problem of deep spherical flaws in a conductor was investigated [45], and it was shown that MicroSQUID could detect these deep flaws when both dc and low-frequency currents were used [46]. Figure 11 shows the experimental contour plots of the magnetic field above a brass bar containing a 4.7 mm radius cavity located 7.9 mm below the surface when 10 Hz, 130 Hz and 200 Hz ac currents were injected into the bar. Note that above 200 Hz the flaw is essentially undetectable. This observation clearly demonstrated the ability of SQUID magnetometry to detect subsurface flaws in cases where the conventional eddy-current technique would not be successful.

In figure 11 the sensitivity of the flaw detection is decreased by raising the operating frequency. This is an example of the skin depth effect, which is important when dealing with ac currents in three-dimensional plates and any relatively thick sample. For a conductor of semi-infinite extent, an induced current decays with depth d beneath the surface as $e^{-d/\delta}$, where δ is the skin depth defined as

$$\delta = \left(\frac{1}{\pi f \mu \sigma}\right)^{1/2} \tag{1}$$

where f is the frequency of the current, μ is the magnetic permeability of the material and σ is the conductivity of the material. Conversely the magnetic signal from a perturbation in uniform current flow below the surface (e.g. a flaw or void in the material interrupting current flow) will decay until it reaches the surface. Hence the skin depth effect limits the maximum depth of detection for any particular flaw size. The skin depth can be increased by lowering the operating frequency and therefore the typical dc–kHz bandwidth of the SQUID is cited as a major advantage for SQUID NDE in the detection of subsurface flaws in conducting structures.

The Vanderbilt group applied the injected current method, with and without a cancellation plate, to samples of interest to the aircraft, electric power generation and fishing industries. An example of subsurface flaws in the aircraft industry is the so-called second-layer crack, which may occur near an aluminium fastener at a lapjoint in an aircraft wing or fuselage. Ma and Wikswo have shown that SQUID magnetometry can be used for detection of these critical flaws [47]. In the power industry, the failure of a generator may be precipitated by local heating in the generator windings due to a region of poor electrical conductivity. Jenks and Wikswo injected current into the individual wires of an actual winding splice and demonstrated from the measured field the distinguishablity of the current path of each wire within the splice [48]. In the fishing industry, the primary optical method of detecting parasites in fish fillets is time consuming, labour intensive and only marginally effective. Jenks and co-workers at Vanderbilt showed [49] that parasites found in certain ocean-going fish have a magnetic signature similar to spherical holes in a conducting plate when current was passed through the fish. This discovery could lead to an automated process for the detection and removal of such parasites.

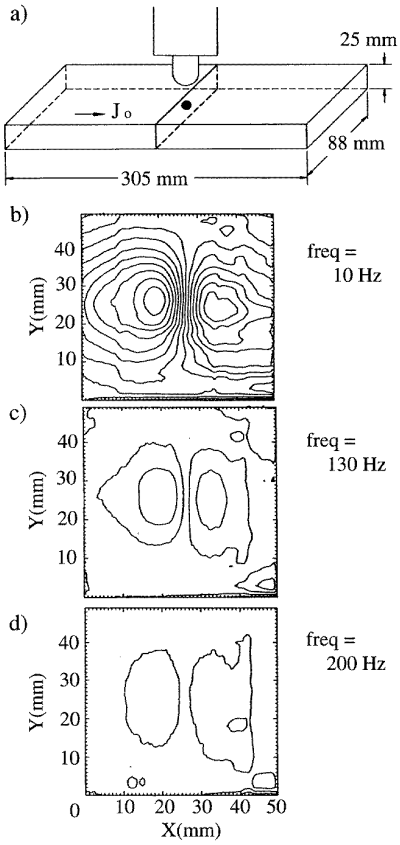

Figure 11. SQUID NDE by the injection current method applied to a thick plate with a subsurface flaw. (a) A thick plate with a 4.7 mm radius spherical cavity centred 7.9 mm below the surface is scanned beneath the SQUID. A 29 mA current is injected into the plate at several frequencies. (b) An isofield contour plot of B_z, produced by a 10 Hz current, above the flawed area of the plate. (c) The same area scanned while injecting a 130 Hz current of the same magnitude. (d) The same area scanned using a 200 Hz current. The contour interval is 200 pT in all three plots. (From [46], with permission.)

4.2. The current induction technique

In the current injection technique described above, establishing a good electrical contact may be difficult or impossible, particularly if the structure is covered by a nonconductive material such as paint or other passivation. In this case, the flow of current in the specimen may be established by inducing eddy currents using a circuit inductively coupled to the sample. Several methods of inducing current will be discussed in this section. These may seem more pedestrian than SQUID technology, but the development of these inducers is very important to the success of this mode of SQUID NDE.

Faraday's law of induction for a linear isotropic medium, which describes the physical mechanism of eddy current induction in metals, is

$$\nabla \times \boldsymbol{J} = -\mu\sigma \frac{\partial \boldsymbol{H}}{\partial t} \tag{2}$$

where σ is the conductivity and μ is the magnetic permeability of the metal. We see that a time-varying

applied magnetic field will induce a current distribution with curl into our medium. These currents with curl are referred to as eddy currents, due to their similarity with the eddies in river water. If the applied magnetic field varies sinusoidally with time, $\boldsymbol{H} = \boldsymbol{H}_0 e^{i\omega t}$, then equation (2) becomes

$$\nabla \times \boldsymbol{J} = -i\omega\sigma\mu\boldsymbol{H}. \quad (3)$$

In qualitative terms, the curl of the eddy currents is out of phase with the inducing field, proportional to the frequency of the applied field, and flows to oppose the *changes* in the applied field with time. The direction of the eddy currents can be determined from the right-hand rule.

The eddy-current inducers discussed here all use a sinusoidal field, although other time variances, notably the step function, have been used with conventional sensors. Conventional eddy-current NDE probes are 1 mm diameter pancake coils with hundreds of turns. They are driven at frequencies from 10 kHz to 10 MHz. They may be used as both the inducer and the sensor in a four-wire configuration. Generally a sinusoidal current is injected into the coil and the voltage across the coil is measured to determine the impedance of the coil. Any conductor near the coil will affect its impedance through mutual inductance, and changes in impedance are then associated with changes in the conductor.

In the first SQUID eddy-current instrument, Capobianco *et al* at the (then) National Bureau of Standards coupled a stationary rf SQUID to a room-temperature probe [50]. This group had already used a rf SQUID magnetometer to measure and map the magnetic field of eddy-current probes [51, 52]. Moulder and Capobianco [53] then used the hybrid system to measure the eddy-current response of some standard simulated flaws made by electrical discharge machining (EDM) notches in a metal plate. In this configuration the SQUID was used as an amplifier for the room-temperature eddy-current probe. It was shown that despite an 80 dB increase in the magnitude of the flaw signal, the eddy-current probe and not the SQUID determines the main features of the signal.

As mentioned above, this type of hybrid system, with normal state components coupled to the SQUID, loses a great deal of the intrinsic advantages of a SQUID system with superconducting pick-up coils. Specifically, the bandwidth does not extend down to dc because of the resistance of the normal state components; the noise in the sensor dominates at low frequency (less than 1 kHz), where the ratio of the inductive reactance to the resistance ($\omega L/R$) of the inductive probe (and hence the signal) is small. Even at high frequency, the white (thermal) noise in the probe is still higher than the SQUID noise. The system may still enjoy a broad dynamic range and the SQUID has been shown to be a good rf amplifier [54]. However, room-temperature, low-impedance current-to-voltage converters can suffice in many applications limited by Johnson noise in the pick-up coil [55, 56].

The vast majority of contemporary eddy-current work uses superconducting pick-up coils that do not compromise the sensitivity or bandwidth of the SQUID. The object under test is generally a metal structure with a simulated flaw. We will now discuss a great deal of work carried out

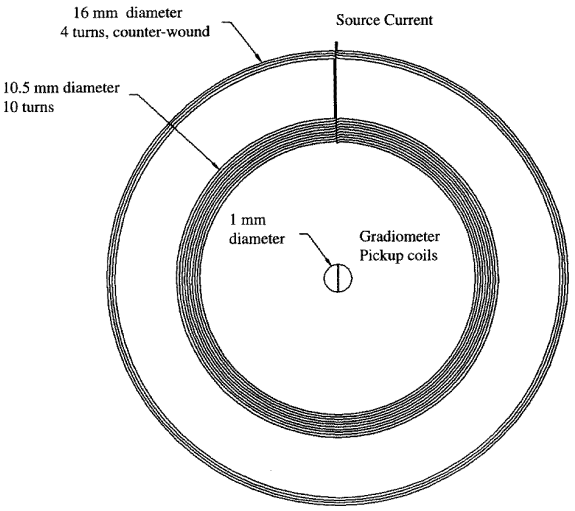

Figure 12. The excitation and pick-up coil configuration for one prototype of the SQM Technology eddy-current probes. The two outermost coils are connected in series and counter-wound to form an excitation coil with a magnetic field profile that is sharper than the inner coil alone. The inner pick-up coil is a planar gradiometer wound to reject any azimuthally symmetric field. The field from the excitation (or source) coil is azimuthally symmetric even in the presence of a uniform conducting plate. This means that the dynamic range of the SQUID can be devoted to flaw detection. (From SQM Technology, with permission, see [58–60].)

by several groups concurrently, with emphasis placed on the interplay between the SQUID, the sample and the current inducing mechanism. This work is of particular interest to the military and civilian aircraft industries who have funded much of the work. Hence the typical samples, particularly in work done in the US, mimic sections of aircraft where conventional NDE is difficult. Obviously the results have implications in other military and civilian industries.

Podney and Czipott proposed [57] a SQUID-based instrument with a counter-wound coil inducer for eddy-current evaluation of materials. Several prototype systems have been constructed and characterized [58] by Podney at SQM Technology. Each uses a counter-wound excitation coil and a planar gradiometer pick-up coil, as shown in figure 12. Eddy currents are induced by the two outer coils. The outermost coil is wound in the opposite sense to the middle coil, and they are connected in series. In the x–y plane just above the two coils, B_z falls to zero more rapidly outside the inner winding than B_z for the inner winding alone. Hence the spatial extent of any eddy currents induced with the two coils is reduced and flaws are more easily localized. The inner coil is a planar gradiometer pick-up coil which is linked to the SQUIDs. This gradiometer pattern, sometimes called a ‘double-D’, is designed so that any field which is symmetric about the azimuthal angle is rejected. The field from the excitation coil is azimuthally symmetric. It remains so even if a uniform conducting sheet is placed in the x–y plane above the coils because the eddy currents would have the same symmetry. The system responds only when the symmetry

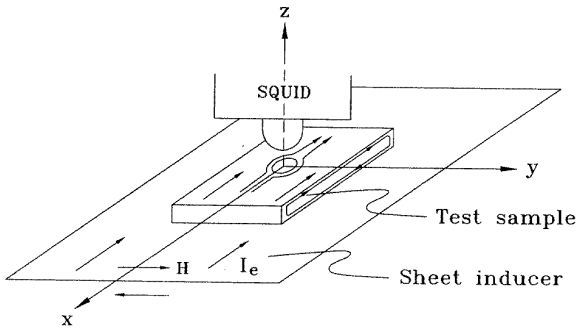

Figure 13. The Vanderbilt sheet inducer for generating uniform eddy currents. The configuration shown here uses a SQUID linked to a pick-up coil sensitive to B_z. Current is injected, in the x direction, into a thin metal sheet beneath the test sample. Above the centre of a large sheet, the inducing field will have only a transverse component B_y. The eddy currents induced into a plate-like sample will be confined essentially to the x direction at all points away from the sample edge. Thus there is negligible B_z above an unflawed sample. When a flaw exists in the sample, shown here centred on (0,0), the eddy currents are perturbed and B_z becomes nonzero. More recent implementations place the inducer between the SQUID and the sample. (Adapted from [61], with permission.)

is broken by a flaw or structural change in the sample. The dynamic range of the SQUID is thus almost wholly devoted to the detection of flaws and the characterization of *changes* in the sample. This is a common theme in SQUID work within and beyond NDE research: configuring the peripheral components so that the SQUID responds only to the signal of interest.

To test the design, Podney [59] fabricated a stack of nine 2024 aluminium plates. Each plate was one millimetre thick and one plate had a one millimetre diameter hole drilled through it. By restacking the plates, he could adjust the depth of this test flaw. The experiments with one prototype demonstrated that the flaw could be detected to a depth of 5 mm. He was also able to map the response of a 'hidden corrosion' sample with 1.4% weight loss. Samples which emulate corrosion damage at a metal interface are of interest to the aircraft and defence industries. Typically two aluminium plates, one with a shallow void, are bonded together with the void at the bond line. The void depth models some percentage of metal loss due to corrosion in that area of the plate. Further work on hidden corrosion samples was done with another prototype [60] which showed that the response of the system was roughly proportional to the depth, and hence the weight loss, of the corrosion holes. The design and variety of the SQM systems will be discussed further in section 8.

The group at Vanderbilt adopted a sheet inducer [61] similar to that used by the magneto-optical inspection (MOI) technique [62]. The sheet inducer, shown in figure 13, is typically large compared to the dimensions of the SQUID pick-up coil, and it carries a nearly uniform current in an x–y plane beneath the SQUID. Thus it approximates an infinite sheet of current in the x–y plane which would have B_y =constant (with a dc current) and $B_z = B_x = 0$ (at all frequencies). This technique induces essentially planar eddy currents in the plate specimen shown in figure 13. Only in the region of the flaw in the plate are the eddy currents perturbed and B_z becomes nonzero. The distribution of the current is more generally a function of the physical properties of the specimen as well as its physical dimensions, and the field at the edge of real world samples is not small. Minimizing B_z from the inducer and the uniform sample allows us to detect the flaw with the SQUID adjusted for greater sensitivity. In addition to the intrinsically low B_z, this technique has one other advantage: the uniform induced currents can be modelled with comparative ease. For cylindrical and tubular samples Podney adopted an analogous long solenoidal inducer [60]. By a similar argument it induces eddy currents in a tube which have almost no magnetic component normal to the surface of the tube. The sheet inducer technique has been used in a number of demonstration experiments, including fatigue cracks [63], second-layer cracks below rivets [60] and hidden corrosion damage [64].

A recent adaptation of coil inducers is the 'double-D' excitation coil. This design is used at Strathclyde [65–67] and (a very similar design) KFA [68, 69] for high-T_c SQUID gradiometric systems. The excitation coil has the same layout as the double-D pick-up coil at the centre of figure 12. The double-D inducer in combination with two high-T_c thin-film SQUIDs (KFA design) is shown in figure 14. The current in the double-D flows through the central bisector then back around the perimeter of the half moons. Thus the field through one D coil is always 180 degrees out-of-phase with the field through the other coil. The two D coils form a closed circuit and the superposed magnetic field lines encircle the centre axis of the coil. At KFA the SQUID gradiometer senses B_z. There is a plane where $B_z = 0$ perpendicular to the excitation coils and both SQUIDs must be aligned to intersect this plane. At Strathclyde, the SQUIDs sense B_x and are parallel to the unperturbed field lines of the excitation coil. In addition, the field outside the coil windings is partially cancelled and the field profile is much sharper than for a single coil of the same radius.

The NDE work done with high-T_c SQUIDs and double-D excitation coils is promising, although the field patterns make interpreting the data rather complex. One of the experiments carried out at Strathclyde [70] used this technology to detect a fatigue crack in a section of an aluminium pressure vessel that was padded with fibreglass in their unshielded laboratory. The resulting map of the field measured by their gradiometer is shown in figure 15(a). This is not an easy problem for conventional NDE: the fibreglass cladding is a poor acoustical link to the aluminium vessel, making ultrasound virtually impossible, and conventional eddy-current systems are designed to work with a smaller separation between metal and probe than is possible here. Limitations of the current technology are also apparent in that the spatial extent of the flaw signal along both axes is determined by the coil diameter (63 mm). Despite the fact that the flaw is roughly 60 mm long and very narrow, the flaw signal covers an area of 120 mm × 60 mm. The sensitivity of the system is low

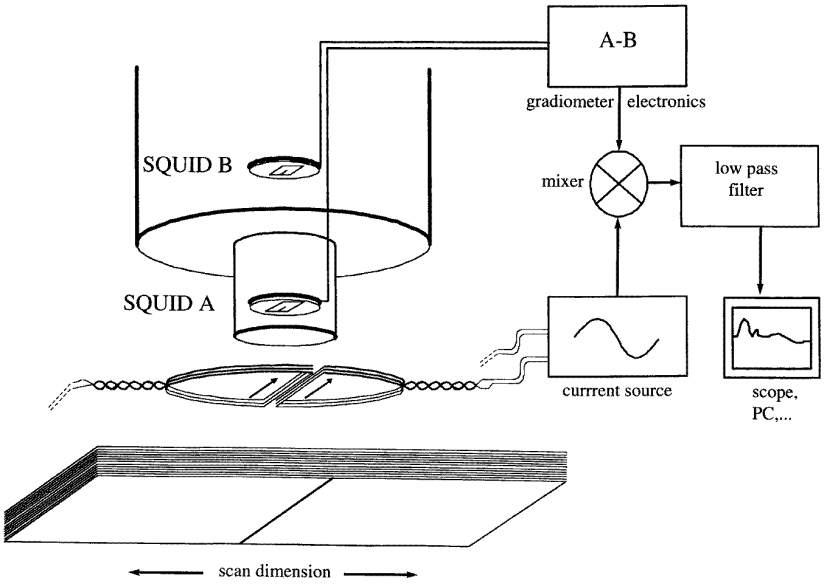

Figure 14. The double-D excitation coil and high-T_c electronic gradiometer configuration (KFA design). The coil is wound so that the currents flowing in the straight section of each D have the same phase. This is indicated by the arrows inside each D coil. There is a plane where $B_z = 0$ perpendicular to the excitation coils and the SQUIDs are aligned to intersect this plane. (From [69], with permission.)

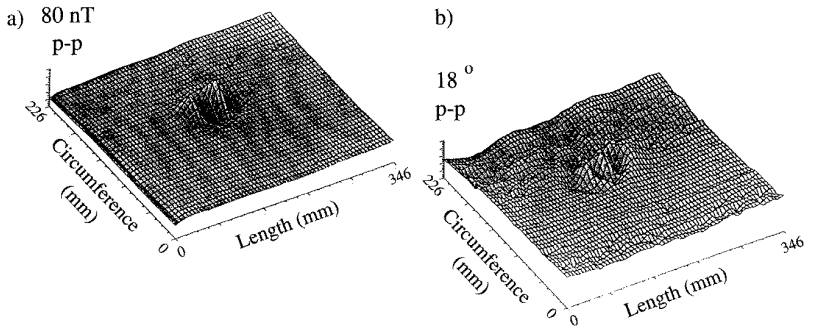

Figure 15. The SQUID response above the surface of a fibreglass-clad aluminium pressure vessel scanned with a high-T_c electronic gradiometer and double-D excitation coil (Strathclyde design). This section of the vessel has a fatigue crack in the aluminium which perturbs the field greatly in the vicinity of (150,150). Notice that although the fatigue crack is oriented along the longitudinal scan direction and is very narrow, the perturbation around the circumference has the same dimension as the inducing coil. (a) The magnitude of the SQUID response. (b) The phase relative to the inducing current. (From [70], with permission.)

compared to low-T_c SQUIDs, and the inducing field is far larger than would be required with a conventional SQUID instrument.

Phase-sensitive detection (PSD) of the eddy-current response of a sample is possible, and the recent explosion of digital lock-in techniques makes it practical at frequencies as low as 10 Hz. A simple explanation of PSD with a lock-in amplifier follows. The fastidious expert may wish to skip to the next paragraph where PSD and SQUIDs are discussed (p 17). PSD can only work with a reference signal. The two main advantages of PSD are the ability to distinguish a relatively small signal from a large broadband noise background and the separation of the sample response into two components which may be the amplitude and phase relative to the reference signal. In SQUID NDE, the excitation signal, an ac current at a particular frequency, ω_s, drives the inducer or excitation coil. The reference signal, which may be a sinusoidal voltage with the same frequency and phase as the excitation current, goes into the lock-in reference port. The digital lock-in generates its own sine wave, with amplitude V_L and frequency ω_L to match the dominant frequency of the reference signal provided. The signal from the sample, i.e. the voltage response of the SQUID, is fed into the lock-in input. The lock-in reference is $V_L \sin(\omega_L t)$, with phase arbitrarily assigned to zero, and the SQUID signal of interest is $V_s \sin(\omega_s t + \Theta_s)$, with phase Θ_s measured relative to the phase of the reference signal. Of course the voltage output of the SQUID will include SQUID noise and environmental interference at many frequencies and phases, but as long as the sample response is linear, the signal of interest will be at the excitation frequency. The lock-in multiplies the SQUID

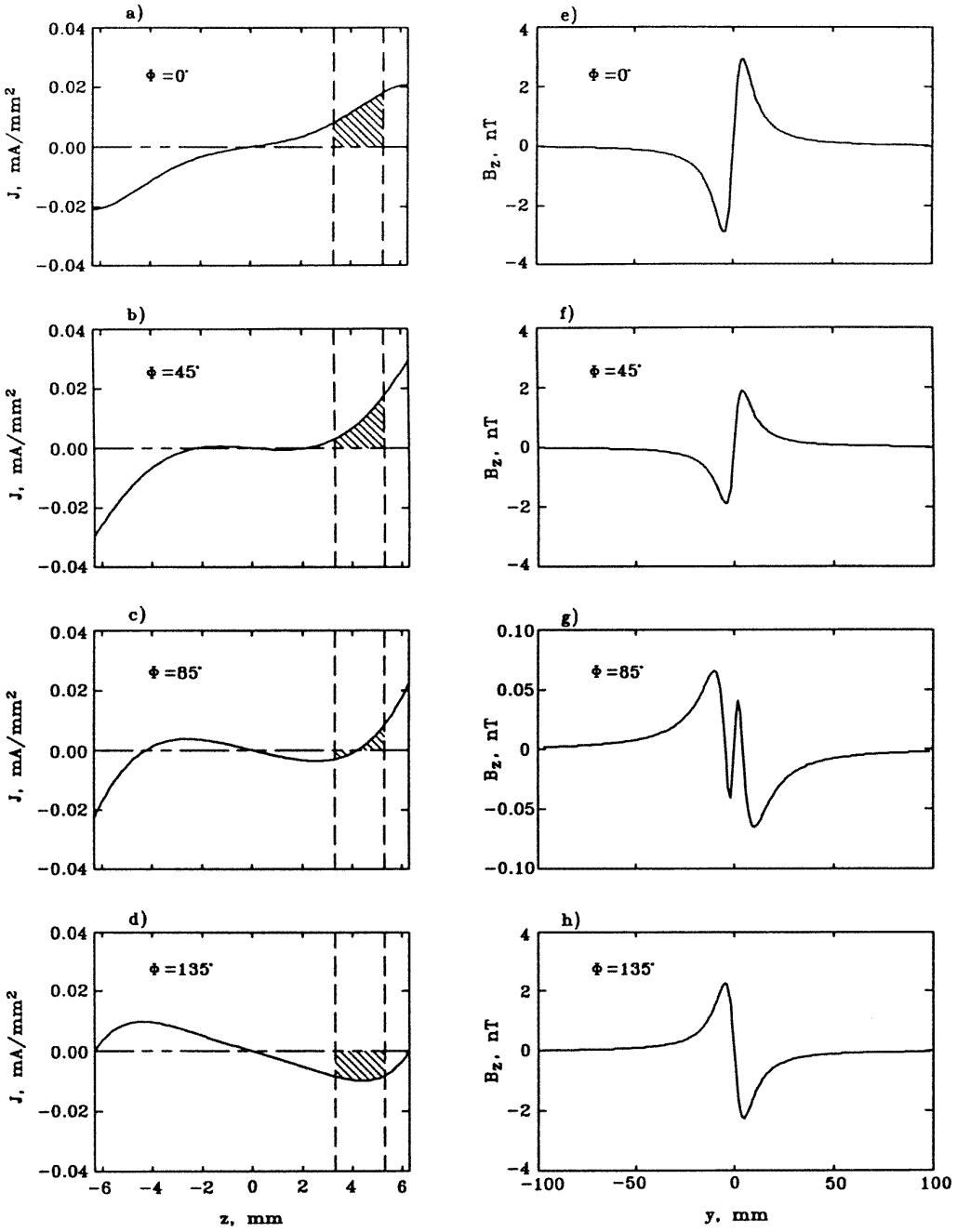

Figure 16. Calculations of the eddy-current density in a plate at a particular phase angle versus depth, and the effect of a disc-shaped flaw. The simulation is for a 12.6 mm thick, unflawed plate with a standard skin depth (equation (1)) of 2.4 mm. Left-hand column: plots of the eddy-current distributions versus phase angle at (a) $\Phi = 0^\circ$, i.e. the eddy current in phase with the excitation field; (b) $\Phi = 45^\circ$; (c) $\Phi = 85^\circ$; (d) $\Phi = 135^\circ$. The horizontal axis is the depth into the plate. The full curves show the magnitude of the eddy currents. The shaded area shows the region in which eddy currents would be perturbed by a disc-shaped void 4 mm in radius, 3 mm thick whose upper surface is located 1 mm below the surface of the plate. Right-hand column: the perturbation at various phase angles in the magnetic field normal to the plate surface due to the flaw. The horizontal axis is the scan length along the surface of the plate. (e) $\Phi = 0^\circ$, the familiar dipole pattern; (f) $\Phi = 45^\circ$, the current density and dipole signature are reduced; (g) $\Phi = 85^\circ$, additional points of inflection in the currents and the corresponding field; (h) $\Phi = 135^\circ$, the dipole is reversed. (From [72], with permission.)

output and the reference signal. The product of any two sine waves of arbitrary frequency is two cosine waves at the difference and sum of the original frequencies. In terms of our signal of interest and the lock-in reference, this would be: $1/2\ V_s V_L \cos[(\omega_s - \omega_L)t + \Theta_s] - 1/2\ V_s V_L \cos[(\omega_s + \omega_L)t + \Theta_s]$. The lock-in then passes this through a low pass filter, which removes all ac components. Only the portion with $\omega_s = \omega_L$ remains: $1/2\ V_s V_L \cos(\Theta_s)$. This is a dc signal proportional to the amplitude of the signal coming from the sample and the cosine of the phase angle

between the SQUID and reference signals. To obtain phase information, the reference signal is also connected to a 90° phase shifter and then another multiplier. The same trick with the excitation signal gives an output of: $1/2\ V_s V_L \sin(\Theta_s)$, again a dc signal. V_L is known and we can now define two quantities: $X = V_s \cos\Theta$ and $Y = V_s \sin\Theta$. These are, respectively, the 'in-phase' or 'real' and 'in-quadrature' or 'imaginary' portions of the signal. We may also solve these for the magnitude, $V_s = (X^2 + Y^2)^{1/2}$, and phase, $\Theta = \tan^{-1}(Y/X)$, of the SQUID signal. Thus two data fields are typically recorded during each eddy-current scan; together they may be called the complex response of the sample. Figure 15, for example, shows the amplitude and phase of the SQUID signal when scanned above a pressure vessel with a fatigue crack. The crack is more apparent in the amplitude of the response, in other cases the signal in the phase channel may be more distinguishable.

Ma and Wikswo at Vanderbilt have shown [71, 72] that the amplitude and phase information can be combined to perform a depth-selective analysis on the sheet-induced eddy current data. They calculated the magnitude and phase, as a function of depth, of the eddy-current density induced in an infinite plate by a uniform ac field parallel to the plate. The depth profiles of eddy-current magnitude J and phase Θ were then converted into depth profiles of the eddy-current component X' at specific phase angles Φ. This is done by simply rotating the conventional X–Y reference frame of the data. The eddy-current component in-phase with the inducing current is $X = J\cos\Theta$ at any particular depth; the eddy current component 30° out-of-phase with the inducing current is $X' = J\cos(\Theta - 30°)$; and for any angle $X'(\Phi) = J\cos(\Theta - \Phi)$. Figure 16, left-hand column, shows the results of calculations for $\Phi = 0°$, 45°, 85°, and 135°. Notice that the current density is always zero at the centre of the plate, which must be true by symmetry, but the depth of the maximum current is a function of Φ. The shaded areas in the plots show the region of current perturbation if the uniform plate contains a cylindrical void. A single scan across the surface of the plate would show the perturbation of B_z due to the cylindrical void shown in the right-hand column. At $\Phi = 0°$, we see the familiar dipolar pattern in the field; at $\Phi = 45°$ the pattern is similar but reduced; at $\Phi = 85°$ the signature of the flaw has changed; and at $\Phi = 135°$ the polarity of the original signature is reversed. This shows the promise of the technique—that subsurface features can be located and distinguished from features in a magnetic image obtained at the surface. The current distribution and field pattern at $\Phi = 85°$ are of particular interest. The current density at this phase angle has three zero crossings instead of one. This leads to two additional extrema in the B_z curve. It is possible to combine the phase at which these two additional extrema are maximized with the conductivity of the material to determine the depth of the flaw. Figure 17 shows this analysis applied to sheet inducer data from a specimen with simulated fatigue cracks under rivets. The specimen, two aluminium plates bolted together with four rivets as shown in figure 17, was scanned using a sheet inducer similar to that shown in figure 13. This specimen is again of special

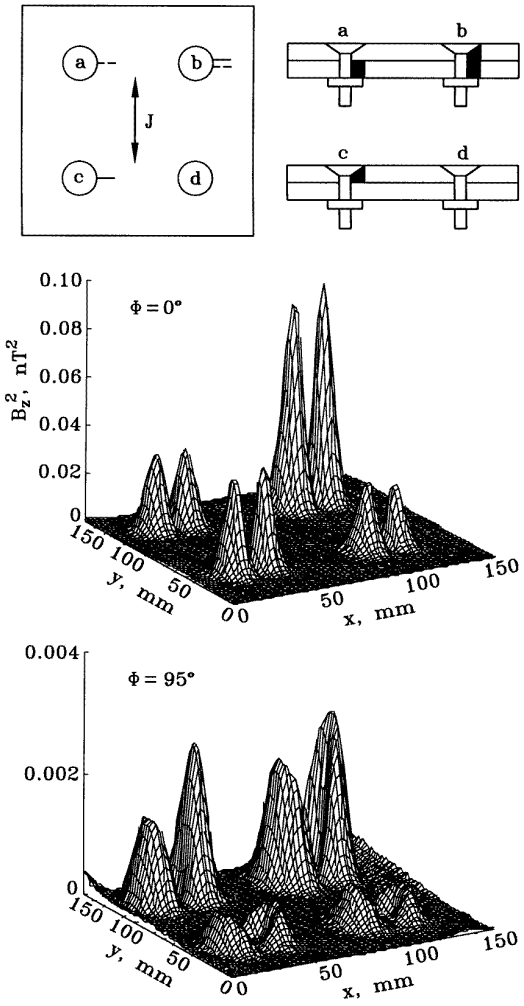

Figure 17. Phase-selective analysis performed on a sample with simulated fatigue cracks. Top: the sample is a pair of 7075-T6 aluminium panels held together by four flat-head bolts. EDM notches are cut in the aluminium under each bolt head to simulate fatigue cracks: (a) one notch in the lower panel; (b) notches in both panels; (c) one notch in the upper panel; (d) no notches. The eddy currents are flowing perpendicular to the direction of the cracks. Centre: the magnetic field response of the specimen at $\Phi = 0°$. The rivets have the familiar dipole signature, which has been squared for clarity. The signal from the fasteners is largest for (b) then (c), (a) and (d). Bottom: the response of the specimen at $\Phi = 95°$. The ratio of the signals from each fastener have changed. At this phase, the signature of the bottom flaw below fastener (a) is far larger than that of the surface flaw of fastener (c). (From [72], with permission.)

interest to the aircraft industry. The dipolar signature of the rivets dominates the field map which has been squared to enhance the clarity of the image but, at $\Phi = 0°$, we see that the rivet with flaws through the top and bottom sheets has the largest signature; the rivet with only a top flaw is smaller; the rivet with only a bottom flaw is smaller still; and the rivet with no flaw is the smallest. If the phase is rotated 95°, the signal from the unflawed rivet is still very small, the rivet with two flaws is still large, but the signal

from the rivet with a bottom flaw is far larger than that from the rivet with the surface flaw.

The additional information obtained with PSD can also be used to enhance system hardware and increase the dynamic range of the SQUID system. Podney [59] gives a brief discussion of the process of 'nulling' the SQUID response to an unflawed sample. This requires that an additional feedback coil be inserted into the circuit in figure 4 where it is inductively coupled to the input coil or the SQUID. This feedback coil is driven by two current sources each at the same frequency as the excitation coil, but one in-phase and one 90° out-of-phase with the excitation signal. Nulling the SQUID is advantageous because none of the passive field minimization procedures discussed above ever achieve perfect cancellation. The system is first used to excite eddy currents in an unflawed section of the sample. The SQUID response to the sample, in-phase and in-quadrature with the excitation signal, can then be cancelled by adjusting the current fed to the feedback coil. Following this, the SQUID can be adjusted to a more sensitive scale (and nulled again if the sample is especially uniform) and the sample scanned.

Note that phase-sensitive detection is possible and common with injected current excitation as well. In fact, Weinstock and Nisenoff recommended it for that purpose in their very early SQUID NDE work [23]. It is emphasized here because it is most often exploited in work with induced currents.

5. Localization of conducting structures and current sources

Finding a hidden structure is sometimes a sufficient challenge in NDE. SQUIDs have been used to find and localize magnetic objects, conducting objects and current sources. The reader is cautioned that a good deal of this work is done by US military contractors interested in direct military applications (e.g. locating targets), which implies that the publication date is delayed a good deal compared to civilian work on subjects (e.g. NDE of aircraft wings) of peripheral interest to the military. As a rule of thumb, one may assume that publication of work with perceived commercial value is delayed 1–2 years by the patent process while publication of work with military value may be delayed 5–15 years.

5.1. Localizing current sources

In their early work, Weinstock and Nisenoff [23] used a second-order biomedical gradiometer to simulate the localization of buried conducting pipes. They injected an ac current into a hollow metallic pipe and measured the resultant magnetic field distribution with a single scan of the gradiometer 1.6 m above the pipe. The axis of the gradiometer was tilted 30° away from the normal, so that when the axis of the gradiometer pick-up coils intersects the axis of the pipe, the detected signal will be near zero. When the gradiometer was directly above the pipe the maximum signal was recorded. Thus with simple trigonometry they could localize the pipe within several centimetres, assuming it ran parallel to the ground.

Localization of current sources has been performed by SQUIDs on many scales, over miles of pipeline and within small objects. Murphy's group at Johns Hopkins University employed SQUID magnetometry to track down the source of stray current on gas pipelines from metro transit systems [73]. The stray current can be a potential source of corrosion, and Murphy's corrosion work is discussed later. It is important to recognize, however, that stray current in gas pipelines can be sufficiently strong [74] that flux-gate gradiometers can be used to detect the magnetic field.

One possible application, on the smallest scale, is the detection of defects in integrated circuits (ICs). This is only possible with SQUID sensitivity as very small test currents are required. As a precursor to this problem, Fagaly [75] reported the use of SQUID magnetometry for detection and localization of electronic timing circuits. His experiment used a standard biomedical dc SQUID gradiometer to measure the magnetic field produced in the vicinity of two commercial watches due to their timing elements. By comparing the SQUID data with the result of an x-ray of the watch, the position of the timing circuit element was easily determined. The capability of high-resolution SQUIDs to localize a current-carrying structure was demonstrated in an early experiment by groups at Vanderbilt and Biomagnetic Technologies Inc. [13] with MicroSQUID, in which magnetic field measurements were made in the close proximity of a wire phantom consisting of 70 wires of 0.28 mm diameter placed side by side. To study the spatial distribution of the magnetic field, a 10 μA, 5 Hz ac current was injected into each wire sequentially. From these measurements, it was concluded that, under the assumption that the source of the field was a long straight line of current in a plane normal to the axis of the pick-up coil, the system is capable of localizing a straight line source to 2.5 μm. This very small number does not hold true in the general problem of an unknown 2D current distribution that was addressed later by Roth and co-workers at Vanderbilt [76] and will be discussed in section 9. For the typical IC and the typical SQUID with 1 mm spatial resolution, the assumption of a long straight wire does not hold true; however, smaller SQUIDs are arriving and a return to the subject is probable.

Zhuravlev and co-workers at the Institute of Radio Engineering and Electronics in Moscow have addressed [77] the problem of SQUID detection of interlayer short circuits on multi-layer chips. They showed that they could localize a single defect to within 2 mm, using a gradiometric system with a minimum lift-off of 6 mm and a pick-up coil diameter of 15 mm.

5.2. Localizing magnetic and conducting objects

Czipott and Podney [78] used an RF SQUID gradiometer to simulate the detection of naval mines. In their first system, which weighs 1400 kg, eight coaxial inducing coils, 2 m in diameter, encircle a gradiometric pick-up coil with a baseline of 23 cm. The source coils, carrying an

ac current, were designed so that they induced essentially zero field in the pick-up coils. With this arrangement, it was shown that the detection sensitivity in water falls as $1/r^7\ \mathrm{e}^{-2r/\delta}$, where r measures the distance from the target and δ is the skin depth, described in equation (1). The system was submerged in seawater and used to detect moving aluminium and iron cylindrical targets. Using a 16.8 Hz excitation signal, they could detect the aluminium target at 9.8 m and the steel target at 5.4 m. The magnetic signal of the steel target, without the eddy-current inducer, was detected at a range of 20 m. A fibreglass target, which has no eddy-current response other than the perturbation of eddy currents in the seawater, as by a void in a conducting medium, was not detected. Czipott and Podney then extended their metal detector for use in a fast moving system, for example with the detector installed in a helicopter [79]. Due to the high speed of the detector, it was shown that a current source with repeated pulses is more appropriate than a single-frequency sinusoidal current. Based on a theoretical model developed for this technique, it was concluded that a prototype system producing pulses 10 ms long and separated by 10 ms, with a peak moment of 2×10^4 A m^2, gives a detection range of 20 m to a target 25 cm in radius.

Clem at the Naval Surface Warfare Center in Panama City, Florida recently presented work [80, 81] on the capabilities of field-deployed SQUID systems for remote sensing of underwater magnetic objects. This sophisticated system uses eight SQUIDs linked to five gradiometers and three magnetometers and is operated at sea onboard a moving platform. This field system is based on a prototype tracking system built in 1975 [82] with eight SQUID channels. From the data reported, it appears that detecting and localizing the sea mines is greatly enhanced by the multiple channels.

6. Active corrosion of metals

Corrosion of metals is the electrochemical process of oxidation. Typically the exposure of metal to an electrolyte, seawater will do, greatly accelerates the process and can lead to reduced structural integrity. In the general case, different parts of a single piece of metal can act as anode and cathode. Current flows between the anodic and cathodic regions and there is a magnetic field associated with this current. Over time, the distribution of anodic and cathodic regions may change. Amongst various techniques for studying corrosion, the analysis of the electrical behaviour of corroded areas is widely used by industry. These techniques conventionally require contact electrodes attached to the specimen for a direct measurement of the electrical parameters of interest. SQUIDs offer a contactless method of detecting ongoing corrosion currents and mapping their distribution. The detection of ongoing corrosion is a totally passive measurement based on the SQUID detecting the field inherent in the sample due to the flow of corrosion current. It should not be confused with the detection of hidden corrosion damage, as discussed above, where the damage could be the result of corrosion that may no longer be ongoing.

John Murphy's group at Johns Hopkins performed early work [73] on the SQUID detection of corrosion currents and developed the magnetically-detected electrochemical impedance spectrum [83] (MEIS) technique usable for field purposes. The MEIS technique is basically a modified version of the electrochemical impedance spectroscopy (EIS) method which measures the ac impedance of a corroded area by applying a small ac voltage and monitoring the resultant current change. In the MEIS technique, measurement of the current change is done indirectly by sensing its associated magnetic field outside the corroded area using a SQUID magnetometer. It was shown that the MEIS technique can provide a contactless method for local assessment of corrosion activity in an isolated segment of a structure; a virtue which previously could not be achieved by the conventional EIS technique. This same group subsequently demonstrated [84] that the signals were strong enough that they could be recorded with a flux-gate gradiometer, thereby obviating the need for SQUIDs in this application.

Bellingham and MacVicar at MIT employed a SQUID gradiometer for studying corrosion processes in nonvoltaic cells [85, 86]. They analysed the magnetic field associated with the flow of dc and ac currents impressed in a simulated corrosion cell. Then they immersed a Zn sample, with ends exposed, into a solution of HCl. In their configuration the SQUID measurement, with the SQUID sensing B_z 2.3 cm above the cell, was dominated by the current flow between the electrodes. With 3 molar HCl, they showed with a single scan over the cell that a current of at least 25 μA was flowing. They were also able to show that the magnetic noise scaled with the corrosion rate. Building on this work, MacVicar's group performed studies [87] on stainless steel and electrodeposition of Zn. Austenitic stainless steel is a particular steel alloy with great corrosion resistance; however, this resistance breaks down if the steel is exposed to temperatures above 500 °C, after which the steel is said to be sensitized. They showed that SQUIDs could detect the onset of corrosion in sensitized steels immersed in an acid bath for several minutes. The electrodeposition of zinc is an important industrial process akin to corrosion. They focused on the possibility of characterizing nonuniform deposition which can lead to the failure of Zn/Ag and Zn/Ni batteries during recharge. Using a flux-gate magnetometer, they showed that the field distributions were different in two extreme cases.

Hibbs and co-workers at Quantum Magnetics Inc. developed a high-resolution SQUID system [88] which allows the pick-up coils to sense either B_z or, by simply rotating a tilted Dewar, the perpendicular component of the field. The system has been used to study corrosion [89] in lapjoints of the aluminium alloy 2024-T3. They imaged the magnetic field normal to one surface of a lapjoint when the opposite surface was exposed to a strong electrolytic solution and found that the corrosion current was concentrated near the rivets. The system was also used in another configuration to compare the low-frequency, magnetic noise power spectral density to the power spectral density recorded by a potentiostat that was connected across two electrodes. It was shown that the correlation was very

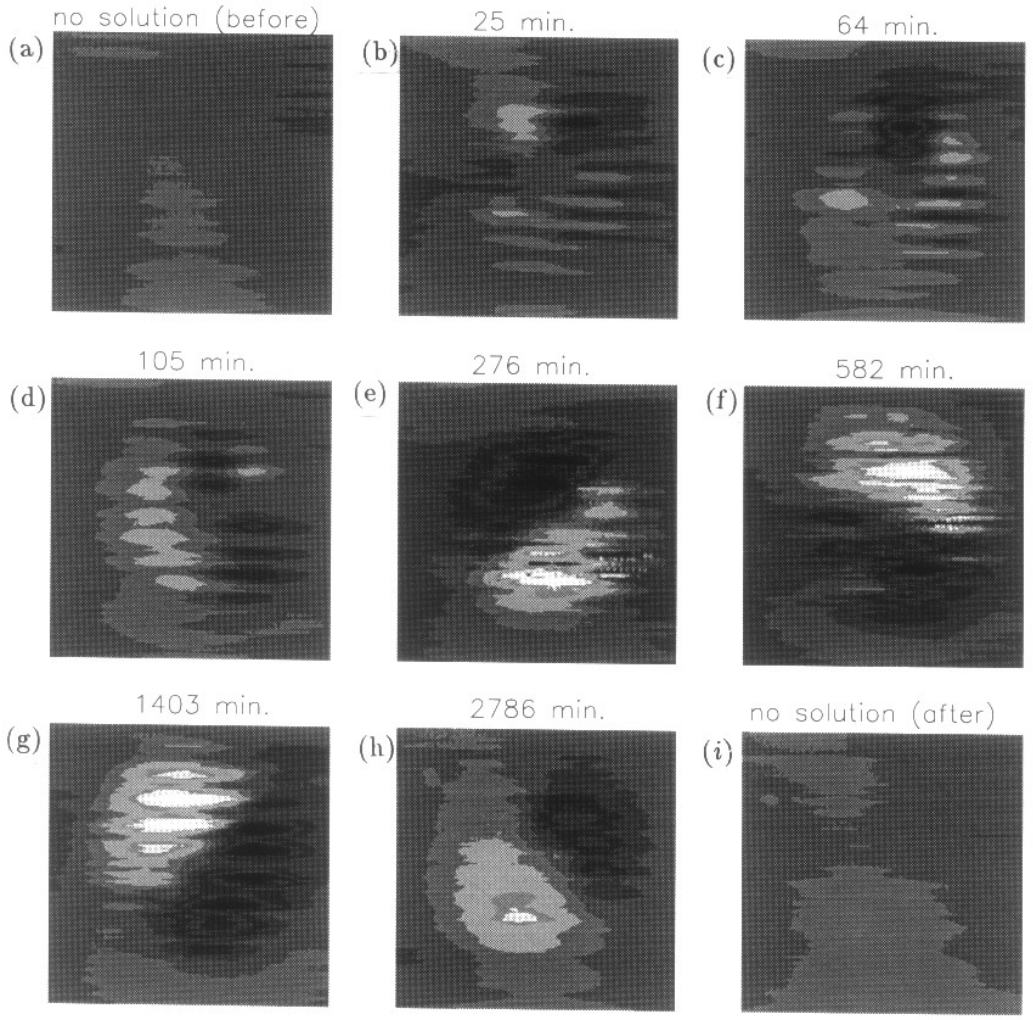

Figure 18. Magnetic images of ongoing corrosion currents at the surface of a 32×32 mm^2 plate of 7075-T6 aluminium alloy immersed in a solution of 3.5% NaCl + 50 ppm Cu^{++}. The image acquisition time for each scan was 18 min and covered an area of 100×100 mm^2 in 1 mm steps. (a) Data taken in air before immersion. (b)–(h) Images during ongoing corrosion. The time interval after immersion, in minutes, for each image was: (b) 25–43; (c) 64–82; (d) 105–123; (e) 276–294; (f) 582–600; (g) 1403–1421; and (h) 2786–2804. (i) Data taken in air following immersion. (From [91], with permission.)

high in the millihertz regime. This demonstrated that the two methods are measuring the same phenomenon, but the potentiostat measures the voltage oscillations of the entire corrosion region while the SQUID is capable of imaging the distribution of current flow.

At Vanderbilt, studies [90–92], of corrosion have focused on determining the signal strength and character above technologically important alloys undergoing active corrosion. Vanderbilt's high-speed scanning stage allows a 100 mm $\times$ 100 mm area to be scanned with a 1 mm step size in 18 min. Thus Li *et al* [90–92] could image the time course of corrosion in a 90 mm diameter corrosion cell over a 24 h period. Figure 18 shows the magnetic field images recorded over time for a square of 7075-T6 aluminium plate sample in a salt solution. Notice that the regions of anodal and cathodal activity change over time. They also demonstrated the detection of 'crevice' corrosion in a ≈ 50 μm gap between aluminium and Plexiglass, designed to simulate inter-layer crevices in aircraft structures.

7. Nonconducting materials

In recent years, ceramic materials and nonmetallic composite materials have been widely used in a variety of structures and components in industry. Amongst existing techniques for monitoring the integrity of such diamagnetic and paramagnetic materials, which include ceramics, plastics and composites, SQUID susceptometry is very promising. The success of this technique in NDE applications was demonstrated by Wikswo and his group at Vanderbilt University [93]. They showed that a high-resolution, sensitive susceptibility imaging system can be used to measure the susceptibility distribution in a nonconducting material for detection and sizing of flaws. This technique is based on the fact that the susceptibility of a flaw in a material normally differs from the rest of the material. In the initial imaging system [94], the spatial distribution of the magnetic field outside the material was obtained with a SQUID magnetometer in conjunction with

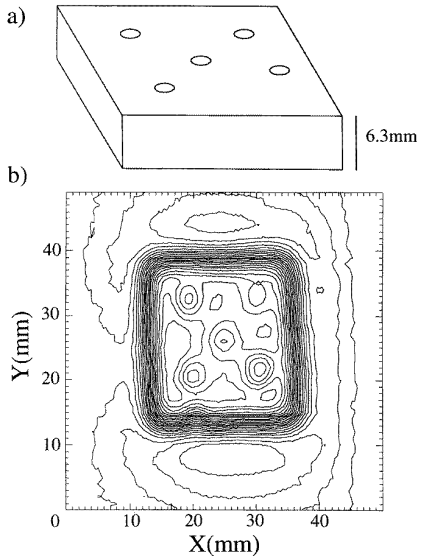

Figure 19. SQUID detection and characterization of two-dimensional flaws in nonconducting materials. (a) Geometry of the one-inch wide Plexiglass sample with several through holes. (b) Contour map of the measured magnetic field with an applied field of 110 μT. The isofield contour interval is 10 pT. (From [93], with permission.)

a pair of Helmholtz coils that applied an essentially uniform field of magnitude 0.3 mT. The field distribution was then inverted using a fast Fourier transform (FFT) algorithm to obtain the susceptibility distribution within the material. It is worth mentioning that SQUID susceptometry had already been employed in biomedical applications [18, 95–97], although no attempt was made to invert the field measurement data to obtain the susceptibility distribution.

In order to demonstrate the capability of the technique in flaw detection and sizing in nonconducting materials, the Vanderbilt group presented three cases. Their first experiment was a two-dimensional problem in which they scanned blocks of Plexiglass containing various holes, as shown in figure 19. They showed that the geometries of the holes at the surface of the sample could be imaged accurately using an appropriate deconvolution algorithm [98]. It was observed that the system is sensitive to susceptibility contrasts as small as 5×10^{-7} (SI) with a spatial resolution of the order of 1 mm.

The second case involved the more general problem of three-dimensional flaws in a nonconducting material. It is well known that any solution to a general 3D inversion from magnetic fields measured on a closed surface to the magnetization distribution enclosed is nonunique. To solve the associated inversion problem, they showed that a solution could be obtained by neglecting the mutual magnetization within the material (which is a correct approximation for most nonferromagnetic materials), by dividing the sample into volume elements termed voxels that each have a constant susceptibility, and by using multiple configurations of field, sample, and magnetometer [99]. The solution, though unique, may be ill-conditioned. They reported that a tomographic reconstruction of the susceptibility distribution in a test sample can be achieved by applying an external magnetic field in different directions, by rotating the sample, or by measuring the magnetic field at different levels. To demonstrate the feasibility of the technique, they carried out a numerical simulation with sixty-four volume elements having susceptibilities of either 2.5×10^{-5} (SI) or 2×10^{-5} (SI) randomly distributed within a cubic sample. In this test, the applied field and the sample were stationary and the field measurements were assumed to have been done at different planes over the surface of the sample. They reported a very close match with the surface voxels and roughly good agreement for the interior voxels, but great sensitivity to noise. This sensitivity to noise can be reduced by utilizing a combination of nonuniform magnetizing fields [100].

The effectiveness of SQUID susceptometry was further demonstrated in a novel NDE technique called surface decoration susceptometry. In this technique, the surface of a nonmagnetic sample is decorated with a ferromagnetic [40, 101] or a superparamagnetic [102] tracer, and a high-resolution magnetometer or susceptometer is used to image the remanent magnetization or susceptibility distribution respectively of the decorated sample. An analysis of the resulting image is then utilized for detection of very fine surface-breaking cracks. The detection sensitivity appears to be limited by applied field strength, SQUID noise, and by the spatial resolution of the sensing coils. *Any* low-frequency application limited by SQUID noise is promising. It generally means that no other magnetic method will work.

A great deal of SQUID work on nonconducting samples has been done in the hope of developing a technique suitable for the NDE of composite materials (e.g fibreglass/epoxy composites like G-10) where traditional electromagnetic and ultrasonic methods are limited. Susceptibility imaging may prove ideal for this application, but workers outside the SQUID field are trying to build in inspectability by 'tagging'. Tagging [103–105] is a process whereby a small quantity of fine magnetic particles is incorporated into the composite matrix before curing. It makes inspection by conventional means possible; however, too many of these tracer particles can degrade the performance of the composite. Jenks and co-workers at Vanderbilt University [106] measured samples of these materials with a desensitized SQUID susceptometer and correlated these measurements with a simple model. They showed that with SQUID NDE, it would be possible to reduce the magnetic content, typically 1–10% by weight, by a factor of at least 1000, i.e. to the point where the effect of tracers on the composite would be negligible.

8. SQUID systems for NDE

The major technological advance that brought SQUID NDE into the realm of imaging flaws and current distributions was the development of the first high-resolution SQUID magnetometer (HRSM) built at Biomagnetic Technologies Inc. (BTI) and Quantum Design for John Wikswo at Vanderbilt University [13]. The novel features of this magnetometer, named MicroSQUID, were small-diameter

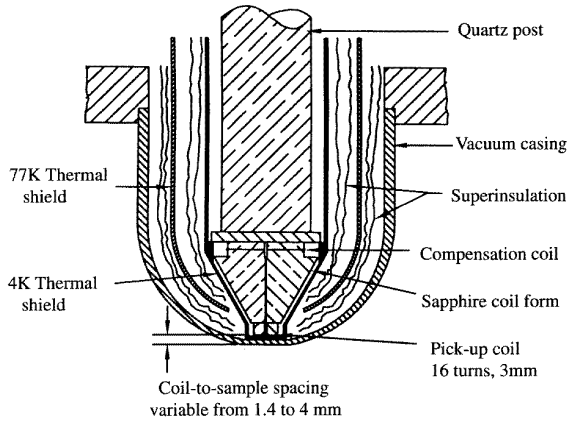

Figure 20. The Dewar tail of the first high-resolution SQUID magnetometer, MicroSQUID. The (then) unconventional design had 3 mm diameter pick-up coils which could be lowered to within 1.5 mm of a room-temperature sample outside the Dewar. The data shown in figures 9–11, 17–19 and 25 were taken with this instrument. (From [13] with permission.)

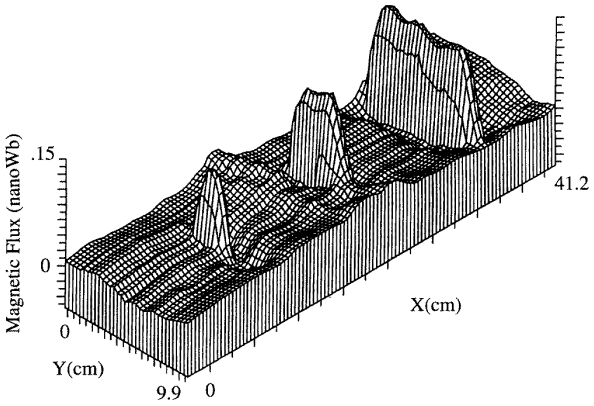

Figure 21. The field distortion detected above a steel plate with a high-resolution SQUID magnetometer. This is to be compared with figure 7(b)—the same plate scanned with an early SQUID system. The coil dimensions and lift-off of the new system are an order of magnitude smaller than in the original. The increase in spatial resolution is apparent as the flaw signals are sharper and distinct from one another. (From [19] with permission.)

pick-up coils (3 mm) and small coil-to-sample spacings (1.5 mm) in comparison to the conventional medical SQUID systems with coil diameters and spacings of the order of 1–2 cm. The overall system is little different from the conventional low-T_c SQUID system shown in figure 5, but the Dewar tail shown in figure 20 maintains a temperature gradient of 300 K across 1.5 mm, and the SQUIDs and pick-up coils are in the vacuum space. The primary advantage of the design is increased spatial resolution. The trade-off for such a design is a relatively large noise (90–100 fT $Hz^{-1/2}$), which could be reduced with improved coupling between the SQUIDs and the pick-up coils. However, it was realized that the reduced coil-to-sample distance and small coil size should provide a larger overall signal-to-noise ratio with a detection resolution that is competitive with that of conventional NDE techniques. MicroSQUID operates best in a magnetic shield [107], and is equipped with a computer-controlled scanning stage [37]. It is not designed for use in magnetically noisy environments or measurements while the Dewar is in motion.

Virtually all SQUID NDE work is now done with high-resolution SQUIDs. The exceptions are work on the magnetomechanical behaviour of steel and remote sensing. The group at Strathclyde has published [19, 108] their development of a high-resolution low-T_c SQUID, as well as a more general account [109] that contains alternate designs. Their system, with a minimum lift-off of 2 mm, has essentially the same spatial resolution as MicroSQUID. The Strathclyde group then repeated one of their early experiments with the high-resolution SQUID. The new system was used to image the steel plate scanned in figure 7 with their original magnetometer; the result is shown in figure 21. Both systems use planar gradiometers. In the original system, the inner coil has an 18 mm diameter, the outer coil has a 41 mm diameter and the lift-off is 51 mm; the corresponding dimensions for the high-resolution system are 2 mm and 4 mm coils and a 12 mm lift-off. A comparison of figures 7 and 21 should demonstrate to the reader the meaning of increased spatial resolution and the benefits of high-resolution SQUIDs. Notice that the length and the width of the flaw signal are more sharply defined. This is due to the combination of sampling the field closer to the source and sampling the field with a smaller coil.

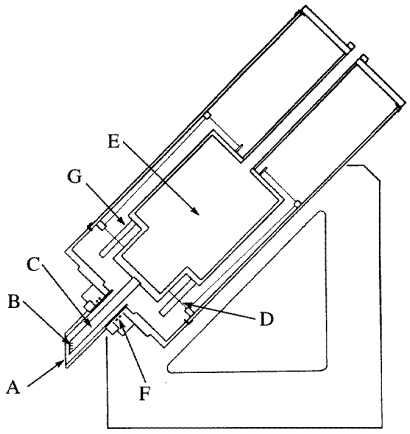

Figure 22. Quantum Design system with the gradiometric axis forming a 45° angle with the Dewar axis. As shown, the gradiometers sense $\Delta B_x/\Delta x$. Rotating the Dewar 180° about its axis allows the gradiometers to sense $\Delta B_z/\Delta z$. The schematic drawing shows the main elements of the design: A, window in the Dewar tail; B, superconducting gradiometers; C, sapphire cold finger; D, Kevlar support wires; E, helium space; F, spring to balance atmospheric pressure; G, SQUID housing. (From [88] with permission.)

Quantum Design has produced [88] a high-resolution SQUID instrument using axial gradiometers with a twist. The tail of the Dewar and the axis of the pick-up coils are offset at a 45° angle from the main axis of the Dewar. Thus if the Dewar is rotated 180° about its axis, the orientation of the gradiometer is changed by 90°. This arrangement is

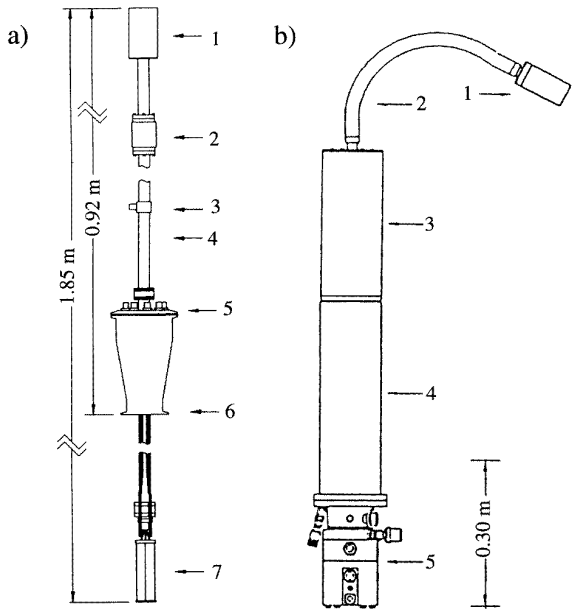

Figure 23. Two SQM prototypes for eddy current NDE. (a) This probe is designed to be inserted into a liquid helium Dewar with the SQUIDs submerged in the helium bath and the pick-up and excitation coils on the top of the probe to scan a sample above the Dewar. From top to bottom we have: 1, the cap which houses a silicon rod, on which the coils are mounted (the coils are separated from the atmosphere by ≈ 3 mm of vacuum space maintained by a thin sapphire window); 2, an expansion joint to adjust the vacuum spacing; 3, vacuum valve; 4, cryogenic umbilical which houses the copper wires used to cool the coils; 5, electrical connections; 6, Dewar fitting; 7, the SQUID housing. (b) This system requires no liquid cryogen and the coils are mounted on a flexible cryogenic umbilical. The system is cooled by a Heliplex HS-4 refrigerator from APD Cryogenics. 1, The cap with pick-up and excitation coils is essentially the same as in (a); 2, a 50 cm long flexible umbilical, by which heat is transported by copper braiding inside a flexible, stainless vacuum tube; 3, SQUID housing mounted onto a Gifford–McMahon refrigerator (4); 5, a valve motor to control the expansion. (From [58] and [60] with permission.)

shown in figure 22, with the gradiometer arranged to sense changes in the horizontal field. If the Dewar is rotated, the gradiometers sense the field in the vertical direction. The gradiometers remain in the superconducting state because the helium bath stays in contact with the cold finger cooling the SQUIDs when the Dewar is rotated. This is a five SQUID system with 1.75 mm diameter, 9.27 mm baseline, axial gradiometers. The minimum separation between the bottom coil of each gradiometer and the sample surface is 1 mm. This instrument has been used mainly for corrosion studies and is discussed in section 6.

Podney at SQM has produced [58–60] several SQUID systems for eddy-current NDE. The inducing and pick-up coil arrangements has been discussed above and vary only in size between the prototypes. The pick-up coil-to-sample spacing is typically 3 to 4 mm. These instruments are unlike the typical SQUIDs used for NDE, and schematics from two recent publications are shown in figure 23. The first probe, figure 23(a), is designed to be dipped into a liquid helium storage Dewar. The rf SQUID housing, at the very bottom of the probe, is submerged in the helium bath. Coaxial copper tubes are used as a cold finger to cool the silicon rod on which the pick-up and inducing coils are mounted at the very top of the probe. To scan a sample, it must be moved in the X–Y plane above the probe with the surface of interest face down. This may seem like an inelegant design, until one realizes that scanning the underside of an aircraft wing is one of the experiments most aspired to in SQUID NDE. The second probe, figure 23(b), is designed to be used with no liquid cryogen and has a flexible cryogenic link between a Gifford–McMahon refrigerator and the pick-up loops. The coil mounting is essentially the same as above. The flexible link is made by running copper braiding through a stainless steel flexible vacuum coupling which is thermally linked to the rf SQUID housing mounted on the Gifford–McMahon expansion stages. A Joule–Thompson expansion stage, not shown, increases the cooling power to 1 W at 4 K. The demonstration that superconducting components can be cooled by metre long, passive thermal links is an important contribution.

The Mechanical Engineering Research Laboratory at Hitachi in Ibaraki, Japan, uses a very small SQUID system [31] built for them by Tristan Technologies, now part of Conductus. The system, which is very much like a miniaturized standard HRSM, has a superconducting magnet coaxial with the pick-up coils. It is mounted on a robot arm and can be scanned in three dimensions, reportedly within ± 0.2 mm. The system is 0.45 m tall, 0.15 m in diameter and weighs only 4 kg (18 inches tall with a 6 inch diameter and weighs under 9 lbs). It is the authors' impression that more than ten SQUID instruments designed for NDE have been shipped to Japan from US companies. The one discussed above is atypical in that it has been described in the open literature. Conductus has built another small system for use with a robot within a nuclear reactor. In addition to six SQUID channels, this system has a 0.1 T dc magnet and a 1 mT ac magnet. No data from this system have been published.

One other type of low-T_c system of interest to the SQUID NDE community is a SQUID mounted on a continuous flow cryostat, such as reported by Kandori and co-workers [110] in Japan. Their 'semi-portable' system was designed for biomagnetic measurements but still has a coil-to-room-temperature spacing of only 5 mm. The advantage of the continuous flow cryostat is that it is cooled only when in use, which is very favourable for any applications requiring a low duty cycle system.

Donaldson and co-workers at Strathclyde have been working on high-T_c SQUID systems for several years. Their developmental work includes a bulk high-T_c instrument without SQUIDs [111], using a bare SQUID to map the field above a current pattern [112], fabrication of high-T_c SQUIDs [113], and using a bare commercial SQUID in a special LN_2 Dewar for eddy-current mapping [114]. Most recently, they have published NDE results using a two-SQUID electronic gradiometer with the sample in motion [66, 67] as well as with the SQUID in motion [115]. The SQUIDs used in the instrument are commercially available Mr. SQUIDs^{TM} from Conductus.

The instrument has a 25 mm baseline axial gradiometer aligned with the horizontal, with an 11 mm minimum lift-off. The magnetic field noise is $\approx$ 100 pT Hz$^{-1/2}$ at 10 Hz and $\approx$ 10 pT Hz$^{-1/2}$ at 10 kHz, in an unshielded environment. It has been used in both eddy current and injected current mode. In other developmental work, they have manufactured [116], modelled [117] and tested single-chip SQUID/gradiometer designs in niobium technology in anticipation of superior fabrication techniques for high-T_c materials becoming available.

The group at KFA in Jülich, Germany, has come into the field from another angle. They developed their high-T_c electronic gradiometers for biomagnetic measurements in unshielded environments, and built bulk [118], thin-film [119] and second-order [120] versions. They then used these systems in a variety of applications [121] including eddy-current work in NDE [68, 69]. Their axial gradiometer has a baseline of 60 mm and a field noise of roughly 500 fT Hz$^{-1/2}$ in the white noise regime. KFA has also developed, with collaborators at ILK in Dresden, a single high-T_c SQUID NDE instrument which will operate in any orientation [122]. The magnetometer system has a field noise in an unshielded environment of 15 pT Hz$^{-1/2}$ at 50 Hz and has been used to detect simulated flaws in a 1.5 mm aluminium plate *above* four unflawed plates by scanning the SQUID along the *bottom* of the lowest unflawed plate. The cold space in this prototype cryostat is insufficient to house one of their electronic gradiometers, but an adaptive cold head is being built for that purpose [123].

SQUID microscopes which operate on cryogenic samples have not yet been discussed, but they are of interest because the technology may lead to room temperature systems of unparalleled spatial resolution. In 1970 Goodman and Deaver at the University of Virginia [124] published a study of the quantized flux states of hollow cylindrical thin films of tin. They scanned the cylinders through a 400 micron magnetometer pick-up coil which was coupled to a bulk rf SQUID. In the early 1980s Rogers at MIT, working with IBM, built a SQUID microscope by coupling a rf SQUID to a wire-wound pick-up coil with a 230 μm inner diameter [125]. The system was used to study flux trapping in niobium thin films at 4.2 K with a resolution of roughly 400 μm. The work at IBM has carried these studies to set a new standard—the image of a single trapped magnetic flux quantum. The IBM low-T_c SQUID microscope [133, 157] has a 10 μm pick-up coil and can map a single magnetic flux quantum Φ_0 trapped in superconducting films, with a system noise of $< 2\Phi_0$ Hz$^{-1/2}$ or 40 pT Hz$^{-1/2}$. This technology has also been furthered at Wellstood's Laboratory at the University of Maryland with a low-T_c SQUID scanning a series of ferromagnetic ink strips in one dimension [126, 127]. The bare dc SQUID used has a 60 μm inner hole side length and the separation between SQUID and sample was held to about 38 μm. The reported system magnetic field noise and spatial resolution are 5.2 pT Hz$^{-1/2}$ at 6 kHz and 66 μm respectively. That system has been emulated [128] in high-T_c by Black, Wellstood and their co-workers at Maryland University and the University of California at Berkeley (UCB). By using a small-area bare $YBa_2Cu_3O_{7-x}$, dc SQUID they achieved a spatial resolution of about 80 μm on a magnetic sample at 77 K, with a noise floor $B_N \approx$ 80 pT Hz$^{-1/2}$ at 1 Hz. Eddy-current instruments [129–131] of similar high-T_c construction have been built and used to image conducting films, at 77 K, with frequencies varying between 26 kHz and 200 GHz. Similar systems [132] have been built elsewhere. This work simultaneously circumvents the lack of high-T_c wire, shields and peripherals and takes a dramatic leap in resolution imaging by making the SQUID loop the limiting dimension in spatial resolution.

There are currently two high-T_c scanning SQUIDs operating on room-temperature samples with spatial resolution of the order of 100 μm. The first, built at the University of Maryland [134], employs a 25 μm thick, single-crystal sapphire window between the SQUID in vacuum and the room-temperature sample. The second, built at UCB [135], has an inverted design (sample above the SQUID) and uses a 3 μm silicon nitride vacuum window [136]. The spatial resolution of these instruments will probably be limited by the window thickness plus window bowing under vacuum and the levelling of the bare SQUID with respect to the window.

For a discussion of the design considerations for magnetic imaging with SQUID microscopes the reader is directed to a recent publication by Wikswo [137].

Another emerging technology of interest to SQUID NDE researchers is digital SQUIDs. Digital SQUIDs attempt to increase the dynamic range of SQUID systems by replacing the conventional room-temperature analogue electronics of the flux-locked loop with either a room-temperature digital signal processor [138–141] (DSP) or an on-chip (4.2 K) integrated Josephson junction feedback circuit that involves flux counting [142–144]. The DSP circuits are being used successfully by a growing number of research groups. The integrated digital SQUID is promising but the technology is still immature and so far underperforms conventional systems, although designs are being examined that will have a sensitivity comparable to that of commercial dc SQUIDs, but with greater dynamic range and slew rate [145]. However, the interest in further development is spurred by the increasing number of channels being used in neuromagnetism and the possibility of true imaging systems for NDE. On-chip feedback would eliminate a great deal of the cost of electronics in systems with more than a hundred sensors and allow for simpler cryogenic design as well, particularly by drastically reducing the number of wires between room temperature and the SQUIDs.

9. Magnetic field modelling and image processing

As in other NDE fields, imaging techniques are useful to facilitate the interpretation of measurement data obtained by SQUID magnetometry. There are essentially two approaches to the processing of SQUID NDE data: flaw detection and field deconvolution into current patterns. We will emphasize flaw detection. We will discuss the work that has been done and the philosophy, if not the

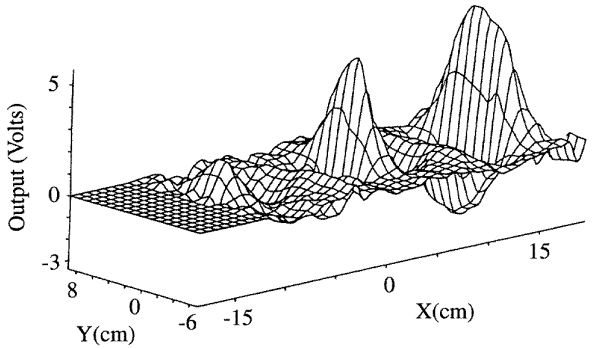

Figure 24. Data from figure 7(b) after a narrow band pass filter has been applied. The flaws in the steel sample are better localized but some information has been removed. (From [17] with permission.)

mathematics, of the methods currently employed in the SQUID NDE community. For a more mathematically detailed review which emphasizes image deconvolution, the reader is referred to a forthcoming work by Wikswo [146].

Flaw detection and sizing is typically the goal of most NDE work and this is likely to be true for SQUID NDE. Mostly conventional methods of enhancing the signature of flaws in a nonuniform background will be discussed in this section. The typical data set in SQUID NDE is a two-dimensional map of a single component of the magnetic field or of the magnetic response to an excitation measured above the surface of a sample. As we have seen, most NDE systems are designed to have a minimal response to unflawed or inactive portions of the sample, so that the dynamic range of the system can be dedicated to characterizing perturbations in a flat (constant value) background. The background is never perfectly flat due to variations in lift-off, sample edge effects, spatial variations in sample thickness or conductivity, imperfect execution of design, environmental noise and, least likely, SQUID noise. The data set is almost certainly digitized and discreetly sampled at regular intervals from the analogue SQUID output. The data may then be filtered in several ways.

To simply enhance the flaw signal or remove unwanted background from the data set, we start with the techniques of digital signal processing or DSP [147, 148]. When the type of flaw is unknown, spatial filtering is used to remove those spatial frequencies in the data which are physically too low or too high to contain significant information about a flaw of limited dimension from a system with limited resolution. The finite impulse response (FIR) filter is one standard technique in DSP for the filtering of unwanted frequencies from a time series data set. These filters function in the spatial domain as well, where the unit of frequency is m^{-1}. FIR filters take the form of a series of constant coefficients which are convolved with the data to emulate in the spatial domain a frequency cut-off in frequency space. These are nonrecursive linear filters so that, having a data set $B(n)$ and filtering, the result $B'(n)$ will take the form

$$B'(n) = c_0 B(n) + c_1 B(n-1) + c_2 B(n-2) + \cdots + c_M B(n-M) \quad (4)$$

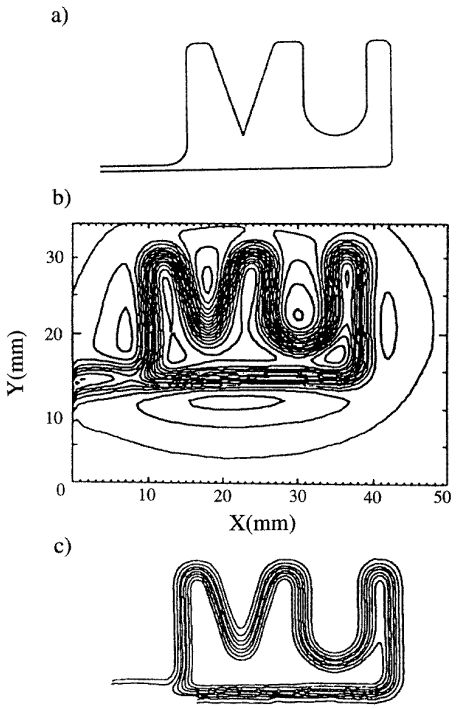

Figure 25. Deconvolution of a two-dimensional magnetic field to obtain the current distribution. (a) The VU current pattern on a printed circuit board. The pattern carried a 100 μA current. (b) A contour plot of the B_z map measured 2.5 mm above the circuit board. (c) The current image calculated from the magnetic field by a Fourier filtering technique. (From [37], with permission.)

where M is the number of coefficients. As an example, the data shown in figure 7 were collected over a steel plate with three transverse grooves at Strathclyde [16]. Figure 24 shows the data after they were band pass filtered between 30 m^{-1} and 40 m^{-1} with a FIR filter. The filtering was performed in one-dimension, along the X, scan, direction. This is a very narrow bandpass filter and the flaw signal has been emphasized at the expense of other information. Notice that the first data points at the beginning of each scan have been replaced by zeros, as is required by the number of coefficients in the filter. A more general linear filter is the infinite impulse response (IIR) filter which has an additional set of coefficients which are convolved with values of $B'(m)$, where $m < n$, to derive $B'(n)$. These have not been applied as extensively in SQUID NDE because they are inherently more difficult to design. The FIR is nonrecursive, its output depends only on previous and current inputs; the output of the IIR also depends on the previous output and therefore is inherently unstable. Using either IIR or FIR filters is typically inferior to performing a discrete Fourier transform (DFT) on the data array, windowing the unwanted frequencies, and transforming back to the data space. The advantage of one-dimensional FIR and IIR filters is that they can be applied in near real time; to begin filtering you only need as many data points as you have coefficients, and hence they are well suited to field instruments. An account of FIR filtering of SQUID data in two dimensions has

been written by Barbosa and co-workers at the Catholic University in Rio de Janeiro [149]. They use low and high pass filters with few coefficients, convolving them many times with the data, and maintain great control over the filtering process. Their results are particularly interesting for high lift-off experiments. Matched filtering is useful in cases where the particular type of flaw is known, e.g. a linear crack or a spherical void. The known flaw signal is convolved with the data and the signal-to-noise ratio of the flaw is enhanced. In early work at Strathclyde [15] on steel plates, it was reported that a matched filter that modelled surface-breaking flaws as magnetic dipoles in steel plates was slightly superior to FIR filters, and both were greatly preferred to the IIR filters which had been tried.

Another technique that shows promise was utilized by Braginski's group at KFA in their work on concrete reinforced with steel rebar [21]. These workers expect to detect many undamaged, equally spaced, rebars in a row, so that as they scan over the concrete they can run an autocorrelation algorithm on their data and identify faults by minimums in the autocorrelation function. This is conceptually equivalent to using a matched filter from a good rebar and identifying signals that are weaker than expected.

Beyond locating flaws, the sizing of flaws from the response of the sample to applied magnetic fields and currents is of prime importance. For this reason, much effort has been devoted to calculating the SQUID response to voids in conductors under various excitation conditions. Knowledge of the flaw signal helps in sizing and locating flaws, in defining possible matched filters, and in the design of the next generation of hardware. The analytic calculation of the magnetic field of spherical voids in a current-carrying plate has been performed by Ma and Wikswo [45]. The finite element method (FEM) has been used at Vanderbilt [3] to model the magnetic field of an F-15 lower wing splice with a small region of hidden corrosion damage, under uniform current flow. The use of the sheet inducer in that laboratory makes the assumption of uniform current flow a plausible one and simplifies the modelling of complex systems. At Strathclyde, modelling work includes the geometry of the inducing mechanism. The FEM was used to model the response to a simple coil inducer [150] of an aluminium plate with a slot cut in the bottom surface. Mc Kirdy and co-workers have successfully used the volume integral method (VIM) to calculate the response of the same slotted plate to a double-D inducer [151]. The VIM can only be used in special cases where both the Green's function of the unflawed sample and the geometry of the flaw are known, but it is computationally much faster than the FEM and has been shown to assist in sizing flaws of the same general shape [152].

In image deconvolution, the objective is to convert noisy magnetic field measurement data into images of the current or magnetization distribution within the sample. The images available in SQUID NDE are typically 2D maps of a magnetic field component B_z at a single height z_0 above the sample. The main constraint this places on inversion methods is that the calculated current distribution pattern is confined to a plane. This equivalent surface current density $\boldsymbol{J}_s(x, y)$ is a useful approximation in cases where the current flow in the physical system is parallel to the imaging plane. For three-dimensional cases, a general inversion algorithm has not yet been developed, and there is no unique solution to the unconstrained, generalized, 3D inverse problem. In two-dimensional cases, the Vanderbilt group showed that a deconvolution technique can solve uniquely for unknown magnetic field sources [153]. This was demonstrated experimentally [37] on the current pattern shown in figure 25. This two-dimensional 'VU' current pattern was created on a printed circuit board. Figure 25 shows a two-dimensional current pattern created on a printed circuit board. The magnetic field was measured 2.5 mm above the board when the pattern carried a 100 μA current, and the current imaged from that field with a Fourier inverse filtering technique is also shown.

The Vanderbilt group has developed several other algorithms based on various numerical techniques. For example, Fourier inverse spatial filtering was employed to determine the current distribution in a conducting plate containing rivets placed in 4 mm diameter holes [154]. In other experiments, they utilized the FEM to compute the current distributions in a superconducting and normal state $YBa_2Cu_3O_{7-x}$, thin film [154]. To investigate the current distribution in flawed conducting tubes, Wikswo's group adopted lead field analysis [101] for inverting the measured magnetic field data. In this experiment, current flowed axially along a 12.1 mm metal tube with a 4 mm diameter hole in the wall of the tube. The radial magnetic field was measured at 3.5 mm above the tube surface and subsequently was inverted to study the effect of the hole on the current distribution on the tube. The reconstructed image clearly shows the presence of the hole.

A review of the inversion techniques mentioned above [155] concludes that each technique has advantages when applied to a particular problem, while it may fail for others. For example, the FEM is appropriate for cases where the solution is to be constrained with boundary conditions [156]. For complex geometries, on the other hand, lead field analysis is numerically simple but requires more computation time and cannot be used with discontinuous sources.

One benefit of the FEM and other modelling work at Strathclyde and Vanderbilt that is not often appreciated is the possibility of visually studying the current flow around flaws in particular structures. In the future we may expect that the design of SQUID magnetometers for NDE tasks in specific industries will be governed more by the complex response of the expected flaws than by optimizing the general performance of the system.

10. Future outlook

The future of SQUID NDE looks very promising. The advent of high-temperature superconductivity, the development of SQUID instruments specifically for NDE, and the application of sophisticated data analysis has greatly enhanced the prospects for getting the field out of the laboratory, into the factory and onto the flight line. That

step is, however, a very large one. An overview of the commercial NDE market and the technologies competing with SQUIDs has been given by Wikswo [3]. Some speculation will now be presented, for the amusement of future SQUID builders, on the possibility of SQUID NDE becoming a commercial technology.

The SQUID has no equal as a sensor of magnetic flux. All other electromagnetic sensors are fundamentally inferior to SQUIDs at frequencies below several kilohertz. The technology necessary to bring this superior tool to bear on the problems of interest in NDE is being developed. There is no reason to doubt that the technology can be developed. The sensitivity of SQUIDs is unparalleled. The SQUIDs can detect fields at frequencies from dc to gigahertz. The dynamic range is large and with the advent of digital SQUIDs may grow even larger. The spatial resolution will continue to improve. There are no insurmountable barriers between SQUIDs being fundamentally the best sensors and the best practical instruments for electromagnetic NDE. However, one crucial component is missing. SQUID NDE needs a customer! Currently nearly all work on SQUID NDE is financed by government or industrial research grants, and promising results are being produced, but that promise will not be fulfilled without innovative people driving the technology and finding that crucial first niche. The field of SQUID NDE presently has a number of innovators, but unless a customer is found, these innovators will disappear.

Let us divide all possible samples into two categories, large and small. The SQUID experts' definition of large is anything that the SQUID must be scanned over; similarly small means anything that can be scanned under the SQUID. In the large category we have aircraft, ships, power plants, oil platforms, bridges, airport runways, the NASA shuttle, production-scale metal stock and many other large items. In the small category we have integrated circuits, aluminium cans, food items, auto parts, glassware and other small objects. Let us define a commercial SQUID NDE instrument as one which can be unpacked and operated without the assistance of a PhD and is bought (not funded) by industry for present needs.

Small items are often ignored, but they are intriguing. The capability exists today to build a linear array with ten SQUIDs into a commercial instrument which could scan a quasi-two-dimensional sample with millimetre resolution. If the item were on an assembly line with a nonmagnetic belt, it could be scanned beneath SQUIDs that were located in a compact magnetic shield right on the line. In the case of small items, very few applications have been tried and very few problems identified by the SQUID community. The perception is that small items are cheaper to replace than inspect so they are of little interest. In fact some critical components are small and SQUID work aimed at nuclear reactor fuel rods [40] and microchips [75, 77] has been performed. Inexpensive small items may also be a possibility provided they can be scanned very quickly. Jenks *et al* [49] recently estimated 1–2 s scan times for detection of parasites in fish fillets, an apparently mundane NDE problem that accounts for approximately one-half the cost of harvesting and marketing certain white fish.

For large item applications, we have identified many problems where present technology is insufficient, with detection of second-layer cracks in aircraft wings and cracks in rebar as prime examples. We have yet to demonstrate that SQUIDs are the answer to any of these problems, but again the results are promising. Within the next five years we should know if any of the current list of possible problems can be solved with SQUID NDE and, just as importantly, cannot be solved by improvements in other NDE technologies. A $40 000 SQUID is not much of a system today, whereas a $40 000 Hall probe would be at the top of the range. A commercial SQUID system for large items may take more than five years to develop; ten years is often quoted as the time for true commercialization of SQUID NDE. Sometimes this is used as a conservative number and sometimes a liberal number—more likely it will be the time from the discovery of the first successful niche to industry standard. The niche must be found first.

Acknowledgments

The preparation of this manuscript has been funded in part by grants from the Electric Power Research Institute and the Air Force Office of Scientific Research. We thank our many friends worldwide who provided us with publications, preprints and illustrations. We are indebted to Cheryl Cosby for her hard work and care in preparing the manuscript, and to Licheng Li for preparing many of the illustrations. We thank Harold Weinstock, Joachim Krause, Sandy Cochran, Leonora Wikswo and Margaret Khayat for their very helpful comments on this manuscript.

References

[1] Weinstock H 1991 A review of SQUID magnetometry applied to nondestructive evaluation *IEEE Trans. Magn.* **27** 3231–6

[2] Donaldson G B 1989 SQUIDs for everything else *NATO ASI Series, Superconducting Electronics* ed H Weinstock and M Nisenoff (New York: Springer) pp 175–207

[3] Wikswo J P Jr 1995 SQUID magnetometers for biomagnetism and nondestructive testing: Important questions and initial answers *IEEE Trans. Appl. Supercond.* **5** 74–120

[4] Cochran A, Donaldson G B, Morgan L N C, Bowman R M and Kirk K J 1993 SQUIDs for NDT: The technology and its capabilities *Br. J. NDT* **35** 173–82

[5] Clarke J 1989 SQUID concepts and systems *NATO ASI Series, Superconducting Electronics* ed H Weinstock and M Nisenoff (Berlin: Springer) pp 87–148

[6] Barone A and Paternò G 1982 *Physics and Applications of the Josephson Effect* (New York: Wiley)

[7] Josephson B D 1962 Possible new effects in superconductive tunnelling *Phys. Lett.* **1** 251–3

[8] Drung D 1996 Advanced SQUID read-out electronics *SQUID Sensors* ed H Weinstock (Dordrecht: Kluwer)

[9] Fagaly R L 1990 Neuromagnetic instrumentation review *Adv. Neurol.* **54** 11–32

[10] Wikswo J P Jr 1978 Optimization of SQUID differential magnetometers *AIP Conf. Proc.* **44** 145–9

[11] Koch R H, Rozen J R, Sun J Z and Gallagher W J 1993 Three SQUID gradiometer *Appl. Phys. Lett.* **63** 403–5

[12] Tavrin Y, Zhang Y, Mück M, Braginski A I and Heiden C 1993 $YBa_2Cu_3O_7$ thin film SQUID gradiometer for biomagnetic measurements *Appl. Phys. Lett.* **62** 1824–6
[13] Buchanan D S, Crum D B, Cox D and Wikswo J P Jr 1989 MicroSQUID: A close-spaced four channel magnetometer *Advances in Biomagnetism* ed S J Williamson *et al* (New York: Plenum) pp 677–9
[14] Bain R J P, Donaldson G B, Evanson S and Hayward G 1985 SQUID gradiometric detection of defects in ferromagnetic structures *SQUID '85, Proc. 3rd Int. Conf. on Superconducting Quantum Devices* ed H D Hahlbohm and H Lübbig (Berlin: deGruyter) pp 841–6
[15] Bain R J P, Donaldson G B, Evanson S and Hayward G 1987 Design and operation of SQUID-based planar gradiometers for non-destructive testing of ferromagnetic plates *IEEE Trans. Magn.* **23** 473–76
[16] Evanson S 1988 The evaluation of a SQUID based noncontact magnetic NDE technique for application to the inspection of offshore steel structure *PhD Thesis* University of Strathclyde, Glasgow, Scotland
[17] Evanson S, Bain R J P, Donaldson G B, Stirling G and Hayward G 1989 A comparison of the performance of planar and conventional second-order gradiometers coupled to a SQUID for the NDT of steel plates *IEEE Trans. Magn.* **25** 1200–3
[18] Wikswo J P Jr, Opfer J E and Fairbank W M 1980 Non-invasive magnetic detection of cardiac mechanical activity: experiment *Med. Phys.* **7** 307–14
[19] Cochran A and Donaldson G B 1992 Improved techniques for structural NDT using SQUIDs *Superconducting Devices and Their Applications* vol 64 ed H Koch and H Lübbig (Berlin: Springer) pp 576–80
[20] Bruno A C, Ewing A P and Wikswo J P Jr 1995 Measurements of surface-breaking flaws in ferromagnetic plates by means of an imaging SQUID susceptometer *IEEE Trans. Appl. Supercond.* **5** 2484–5
[21] Sawande G, Straub J, Krause H-J, Bousack H, Neudert G and Ehrlich R 1995 Signal analysis methods for the remote magnetic examination of prestressed elements *Proc. Int. Symp. on Non-Destructive Testing in Civil Engineering (Berlin, September 1995)* (Berlin: DGZP EV)
[22] Weinstock H and Nisenoff M 1985 Nondestructive evaluation of metallic structures using a SQUID gradiometer *SQUID '85, Proc. 3rd Int. Conf. on Superconducting Quantum Devices* ed H D Hahlbohm and H Lübbig (Berlin: deGruyter) pp 843–7
[23] Weinstock H and Nisenoff M 1986 Defect detection with a SQUID magnetometer *Review of Progress in QNDE* vol 5 ed D O Thompson and D Chimenti (New York: Plenum) pp 669–704
[24] Mignogna R B and Chaskelis H H 1989 Investigation of deformation using SQUID magnetometry *Review of Progress in QNDE* vol 8 ed D O Thompson and D Chimenti (New York: Plenum) pp 551–8
[25] Mignogna R, Browning V, Gubser D U, Schechter R S, Simmonds K E and Weinstock H 1993 Passive nondestructive evaluation of ferromagnetic materials during deformation using SQUID gradiometers *IEEE Trans. Appl. Supercond.* **3** 1922–5
[26] Weinstock H, Mignogna R B, Schechter R S and Simmonds K E 1992 An improved system for the nondestructive evaluation of steel *Superconducting Devices and Their Applications* ed H Koch and H Lübbig (Berlin: Springer) pp 572–5
[27] Banchet J, Jouglar J, Vuillermoz P-L, Waltz P and Weinstock H 1995 Evaluation of stress in steel via SQUID magnetometry *Review of Progress in QNDE* vol 14 ed D O Thompson and D Chimenti (New York: Plenum) pp 1675–82
[28] Banchet J, Jouglar J, Vuillermoz P-L, Waltz P and Weinstock H 1995 Magnetomechanical behavior of steel via SQUID magnetometry *IEEE Trans. Appl. Supercond.* **5** 2486–9
[29] Weinstock H, Erber T and Nisenoff M 1985 Threshold of Barkhausen emission and onset of hysteresis in iron *Phys. Rev.* B **31** 1535–53
[30] Donaldson G B, Evanson S, Otaka M, Shimzu T and Takaku K 1990 Use of SQUID magnetic sensor to detect aging effects in Duplex stainless steel *Br. J. NDT* **32** 238–40
[31] Otaka M, Enomoto K, Hayashi M, Sakata S and Shimizu S 1994 Detection of fatigue damage in stainless steel using a SQUID sensor *The American Society of Mechanical Engineers: Determining Material Characterization* PVP-vol 276, book no G00844 ed J C Spanner Jr pp 113–7
[32] Pappas D P, Prinz G A and Ketchen M B 1994 Superconducting quantum interference device magnetometry during ultrahigh vacuum growth *Appl. Phys. Lett.* **65** 3401–3
[33] Spagna S, Sager R E and Maple M B 1995 Ultrahigh vacuum compatible superconducting quantum interference device magnetometer system for studies of magnetic thin films *Rev. Sci. Instrum.* **66** 5570–6
[34] Libby H L 1971 *Introduction to Electromagnetic Nondestructive Test Methods* (New York: Wiley)
[35] Jenks W G, Bouma P, Rey C M, Testardi L R and Vinals J 1992 Measuring the homogeneity of ceramic superconductors by eddy current probing *Rev. Sci. Instrum.* **63** 3417–21
[36] Ma Y P, Staton D J, Sepulveda N G and Wikswo J P Jr 1991 Imaging flaws with a SQUID magnetometer array *Review of Progress in QNDE* vol 10A, ed D O Thompson and D Chimenti (New York: Plenum) pp 979–86
[37] Wikswo J P Jr, van Egeraat J M, Ma Y P, Sepulveda N G, Staton D J, Tan S and Wijesinghe R S 1990 Instrumentation and techniques for high resolution magnetic imaging *Digital Image Synthesis and Inverse Optics* ed A F Gmitro *et al SPIE Proc.* **1351** 438–71
[38] Ma Y P and Wikswo J P Jr Magnetic fields from flaws in thick current carrying plates in preparation
[39] Wikswo J P Jr, Sepulveda N G, Ma Y P, Henry W P, Staton D J and Crum D B 1993 An improved method for magnetic identification and localization of cracks in conductors *J. Nondestr. Eval.* **12** 109–19
[40] Hurley D C, Ma Y P, Tan S and Wikswo J P Jr 1993 Imaging of small defects in nonmagnetic tubing using a SQUID magnetometer *Res. Nondestr. Eval.* **5** 1–29
[41] Sepulveda N G, Staton D J and Wikswo J P Jr 1992 A mathematical analysis of the magnetic field produced by flaws in two-dimensional current-carrying conductors *J. Nondestr. Eval.* **11** 89–101
[42] Gans R R and Rose R M 1993 Crack detection in conducting materials using SQUID magnetometry *J. Nondestr. Eval.* **12** 199–207
[43] Ma Y P and Wikswo J P Jr The magnetic field produced by a elliptical flaw in a current carrying plate, in preparation
[44] Ma Y P and Wikswo J P Jr The magnetic field produced by a cylindrical flaw with finite depth in a thick current carrying plate, in preparation
[45] Ma Y P and Wikswo J P Jr The magnetic field produced by a spherical flaw inside a thick current carrying plate, in preparation
[46] Ma Y P and Wikswo J P Jr 1992 Detection of deep flaws inside a conductor using a SQUID magnetometer *Review of Progress in QNDE* vol 11 ed D O Thompson and D Chimenti (New York: Plenum) pp 1153–9
[47] Ma Y P and Wikswo J P Jr 1993 Imaging subsurface defects using a SQUID magnetometer *Review of Progress in QNDE* vol 12(A) ed D O Thompson and D Chimenti (New York: Plenum) pp 1137–43
[48] Jenks W G and Wikswo J P Jr 1995 SQUID

magnetometers for electromagnetic NDE in the electrical power industry *EPRI Topical Workshop: Electromagnetic NDE Applications in the Electric Power Industry (Charlotte, NC, USA, 1995)* (Charlotte, NC: EPRI)

[49] Jenks W G, Bublitz C G, Choudhury G S, Ma Y P and Wikswo J P Jr 1996 Detection of parasites in fish by superconducting quantum interference device magnetometry *J. Food Sci.* **61** 865–9

[50] Capobianco T E, Moulder J C and Fickett F R 1986 Flaw detection with a magnetic field gradiometer *Proc. of the 15th Symp. on NDE 1986 (NDE Testing Information Analysis Center, San Antonio*) ed D W Moore and G A Matzkanin p 15

[51] Fickett F R and Capobianco T E 1985 Magnetic field mapping with a SQUID device *Review of Progress in QNDE* vol 4 ed D O Thompson and D Chimenti (New York: Plenum) pp 401

[52] Capobianco T E, Fickett F R and Moulder J C 1986 Mapping of eddy current probe fields *Review of Progress in QNDE* vol 5 ed D O Thompson and D Chimenti (New York: Plenum) pp 705–11

[53] Moulder J C and Capobianco T E 1987 Detection and sizing of surface flaws with a SQUID-based eddy current probe *J. Res. Nat. Bur. Stand.* **92** 27–33

[54] Hilbert C and Clarke J 1985 DC SQUIDs as radiofrequency amplifiers *J. Low Temp. Phys.* **61** 263–80

[55] Wikswo J P Jr, Samson P C and Giffard R P 1983 A low-noise, low input impedance amplifier for magnetic measurements of nerve action currents *IEEE Trans. Biomed. Eng.* **30** 215–21

[56] van Egeraat J M and Wikswo J P Jr 1992 A low-cost biomagnetic current probe system for the measurement of action currents in biological fibres *Biomagnetism: Clinical Aspects* ed M Hoke *et al* (Amsterdam: Elsevier) pp 895–9

[57] Podney W N and Czipott P V 1991 An electromagnetic microscope for eddy current evaluation of conductive materials *IEEE Trans. Magn.* **27** 3241–4

[58] Podney W N 1993 A superconducting electromagnetic microscope for eddy current evaluation of materials *Review of Progress in QNDE* vol 13 ed D O Thompson and D Chimenti (New York: Plenum) pp 1947–54

[59] Podney W N 1993 Performance measurements of a superconductive microprobe for eddy current evaluation of subsurface flaws *IEEE Trans. Appl. Supercond.* **3** 1914–7

[60] Podney W N 1995 Eddy current evaluation of airframes using refrigerated SQUIDs *IEEE Trans. Appl. Supercond.* **5** 2490–2

[61] Ma Y P and Wikswo J P Jr 1993 Imaging subsurface defects using SQUID magnetometers *Review of Progress in QNDE* vol 12 ed D O Thompson and D Chimenti (New York: Plenum) pp 1137–43

[62] Fitzpatrick G L, Thome D K, Skaugset R L and Shih E Y C 1993 The present status of magneto-optic eddy current imaging technology *Review of Progress in QNDE* vol 12 ed D O Thompson and D Chimenti (New York: Plenum) pp 617–24

[63] Wikswo J P Jr, Ma Y P, Sepulveda N G, Staton D J, Tan S and Thomas I M 1993 Superconducting magnetometry: A possible technique for aircraft NDE *SPIE Proc. on Nondestructive Testing of Aging Aircraft* vol 2001 ed M T Valley *et al* pp 164–90

[64] Ma Y P and Wikswo J P Jr 1994 SQUID eddy current techniques for detection of second layer flaws *Review of Progress in QNDE* vol 13 ed D O Thompson and D Chimenti (New York: Plenum) pp 303–9

[65] Cochran S, Donaldson G B, Carr C, McKirdy D McA, Walker M E, Klein U, McNab A and Kuznik J 1995 Recent progress in SQUIDs as sensors for electromagnetic NDE *Nondestructive Testing of Materials* ed R Collins *et al* (Amsterdam: IOS) pp 53–64

[66] Kuznik J, Carr C, Cochran A, Morgan L N C and Donaldson G B 1995 First order electronic gradiometry with simple HTS SQUIDs and optimised electronics *Appl. Supercond. 1995* ed D Dew-Hughes (Bristol: IOP) pp 1499–502

[67] Cochran A, Kuznik J, Carr C, Morgan L N C and Donaldson G B 1995 Experimental results in non-destructive evaluation with HTS SQUIDs *Appl. Supercond. 1995* ed D Dew-Hughes (Bristol: IOP) pp 1511–4

[68] Tavrin Y, Krause H-J, Wolf W, Glyantsev V, Schubert J, Zander W and Bousack H 1996 Eddy current technique with high temperature SQUID for nondestructive evaluation of nonmagnetic metallic structures *Cryogenics* **36** 83–6

[69] Tavrin Y, Krause H-J, Wolf W, Glyantsev V, Schubert J, Zander W, Haller A and Bousack H 1995 Eddy current technique with HTS SQUID gradiometer for non-destructive evaluation of nonmagnetic metallic structures *Appl. Supercond. 1995* ed D Dew-Hughes (Bristol: IOP) pp 1519–20

[70] Cochran A, Donaldson G B, Carr C, McKirdy D McA, Walker M E, Klein U, Kuznik J and McNab A 1996 Advances in the theory and practice of SQUID NDE *Review of Progress in QNDE* vol 15 ed D O Thompson and D Chimenti (New York: Plenum) pp 1151–8

[71] Ma Y P and Wikswo J P Jr 1994 Depth-selective SQUID eddy current techniques for second layer flaw detection *Review of Progress in QNDE* ed D O Thompson and D Chimenti (New York: Plenum) pp 303–9

[72] Ma Y P and Wikswo J P Jr 1995 Techniques for depth-selective, low-frequency eddy current analysis for SQUID-based nondestructive testing *J. NDE* **14** 149–67

[73] Murphy J C, Srinivasan R and Lillard R S 1988 Magnetic corrosion sensing on larger or inaccessible structures *Proc. Int. Workshop on NDE for Performance of Civil Structures (Los Angeles, 1988)* ed M S Agababian and S F Masri pp 361–76

[74] Murphy J C, Srinivasan R and Lillard R S 1989 Magnetometer-based measurements of stray current distribution on cathodically protected gas transmission pipeline *Review of Progress in QNDE* vol 8 ed D O Thompson and D Chimenti (New York: Plenum) pp 2149–56

[75] Fagaly R L 1989 SQUID detection of electronic timing circuits *IEEE Trans. Magn.* **25** 1216–8

[76] Roth B J, Sepulveda N G and Wikswo J P Jr 1989 Using a magnetometer to image a two-dimensional current distribution *J. Appl. Phys.* **65** 361–72

[77] Zhuravlev E Yu, Bakharev A A, Matlashov A N, Slobodchikov V Yu, Velt I D, Nikulin S L and Kalashnikov R V 1992 Application of DC-SQUID magnetometers for nondestructive testing of multilayer electronic cards *Superconducting Devices and Their Applications* ed H Koch and H Lübbig (Berlin: Springer) pp 581–3

[78] Czipott P V and Podney W N 1989 Use of a superconductive gradiometer in an ultrasensitive electromagnetic metal detector *IEEE Trans. Magn.* **25** 1204–7

[79] Czipott P V and Podney W N 1991 Pulsed operation of a superconductive electromagnetic gradiometer *IEEE Trans. Magn.* **27** 2971–4

[80] Clem T R 1995 Superconducting magnetic sensors operating from a moving platform *IEEE Trans. Appl. Supercond.* **5** 2124–8

[81] Clem T R 1996 *SQUID Sensors* ed H Weinstock (Dordrecht: Kluwer) to be published

[82] Wynn W M, Frahm C P, Carroll P J, Clark R H, Wellhoner J, and Wynn M J 1975 Advanced superconducting gradiometer/magnetometer arrays and a novel signal processing technique *IEEE Trans. Magn.* **11** 701–7

[83] Murphy J C, Hartong G, Cohn R F, Moran P J, Bundy K and Scully J R 1988 Magnetic field measurement of corrosion processes *J. Electrochem. Soc.* **135** 310–3
[84] Srinivasan R, Murphy J C, Schroebel C B and Lillard R S 1990 Corrosion detection on underground gas pipeline by magnetically assisted AC impedance *Corrosion '90* no 406 *Proc. 45th NACE Conf. (Las Vegas, NV)*
[85] Bellingham J G, MacVicar M L A, Nisenoff M and Searson P C 1986 Detection of magnetic fields generated by electrochemical corrosion *J. Electrochem. Soc.* **133** 1753–4
[86] Bellingham J G, MacVicar M L A, and Nisenoff M 1987 SQUID technology applied to the study of electrochemical corrosion *IEEE Trans. Magn.* **23** 477–9
[87] Misra M, Lordi S and MacVicar M L A 1991 NDE applications of SQUID magnetometry to electrochemical systems *IEEE Trans. Magn.* **27** 3245–8
[88] Hibbs A D, Saeger R E, Cox D W, Aukerman T H, Sage T A and Landis R S 1992 A high-resolution magnetic imaging system based on a SQUID magnetometer *Rev. Sci. Instrum.* **63** 3652–8
[89] Hibbs A, Chung R and Pence J S 1994 Corrosion measurements with a high resolution scanning magnetometer *Review of Progress in QNDE* vol 13, ed D O Thompson and D Chimenti (New York: Plenum) pp 1955–62
[90] Li D, Ma Y P, Flanagan W F, Lichter B D and Wikswo J P Jr 1994 The use of superconducting magnetometry to detect corrosion in aircraft alloys *Proc. Tri-Service Conf. on Corrosion* (Washinton, DC: Department of Defense) pp 335–46
[91] Li D, Ma Y P, Flanagan W F, Lichter B D and Wikswo J P Jr 1995 Detection of *in situ* active corrosion by a SQUID magnetometer *J. Min. Metals Mater.* **47** 36–9
[92] Li D, Ma Y P, Flanagan W F, Lichter B D and Wikswo J P Jr 1996 Application of superconducting magnetometry in the study of aircraft aluminum alloy corrosion *Corrosion* **52** 219–31
[93] Wikswo J P Jr, Ma Y P, Sepulveda N G, Tan S, Thomas I and Lauder A 1993 Magnetic susceptibility imaging for nondestructive evaluation *IEEE Trans. Appl. Supercond.* **3** 1995–2002
[94] Ma Y P, Thomas I M, Lauder A and Wikswo J P Jr 1993 A high resolution imaging susceptometer *IEEE Trans. Appl. Supercond.* **3** 1941–4
[95] Ross D, Hoare A, Samadian V and Milville D 1987 SQUID measurements and computational modelling of a simple thorax phantom *Biomagnetism '87* ed K Atsumi *et al* (Tokyo: Tokyo Denki University Press) pp 402–5
[96] Brittenham G M, Farrell D E, Harris J W, Feldman E S, Danish E H, Muir W A, Tripp J H and Bellon E M 1982 Magnetic-susceptibility measurement of human iron stores *New England J. Med.* **307** 1671–5
[97] Bastuscheck C M and Williamson S J 1985 Technique for measuring the ac susceptibility of portions of the human body or other large objects *J. Appl. Phys.* **58** 3896–906
[98] Thomas I M, Ma Y P, Tan S, and Wikswo, J P Jr 1993 Spatial resolution and sensitivity of magnetic susceptibility imaging *IEEE Trans. Appl. Supercond.* **3** 1937–40
[99] Sepulveda N G, Thomas I M and Wikswo J P Jr 1994 Magnetic susceptibility tomography for three-dimensional imaging of diamagnetic and paramagnetic objects *IEEE Trans. Magn.* **30** 5062–9
[100] Parente Ribero E, Wikswo J P Jr, Costa Ribeiro P and Szczupak J 1996 Magnetic susceptibility tomography with nonuniform field *Proc. 10th Int. Conf. on Biomagnetism (Santa Fe, NM, USA) 1996*
[101] Hurley D C, Ma Y P, Tan S and Wikswo J P Jr. 1993 Imaging of small defects in nonmagnetic tubing using a SQUID magnetometer *Res. Nondestr. Eval.* 1–29
[102] Thomas I M, Ma Y P, and Wikswo J P Jr 1993 SQUID NDE: Detection of surface flaws by magnetic decoration *IEEE Trans. Appl. Supercond.* **3** 1949–52
[103] Clark W G and Shannon R E 1990 Tagging lets you test the untestable *Adv. Mater. Proc.* **137** 59–69
[104] Sun F P, Liang C, Rogers C A and Vick L 1993 Magnetic activation of embedded sensory particles in active tagging interrogation of adhesive bonding *Proc. SPIE* **1918** 400–9
[105] Clark W G Jr 1993 Magnetic particle tagging for improved material diagnostics *Proc. Recent Advances in Adaptive and Sensory Materials and Their Applications* ed C A Rogers and R C Rogers (PA: Technomic) pp 274–84
[106] Jenks W G, Ma Y P, Ribeiro E P and Wikswo J P Jr SQUID NDE of composite materials with magnetic tracers, in preparation
[107] Ma Y P and Wikswo J P Jr 1991 A magnetic shield for wide-band width magnetic measurements for nondestructive testing and biomagnetism *Rev. Sci. Instrum.* **62** 2661–4
[108] Cochran A, Donaldson G B, Evanson S and Bain R J P 1993 First-generation SQUID based nondestructive testing system *IEE Proc.* A **140** 113–20
[109] Cochran A, Donaldson G B, Morgan L N C, Bowman R M and Kirk K J 1993 SQUID for NDT: the technology and its capabilities *Br. J. NDT* **35** 173–82
[110] Kandori A, Ueda M, Ogata H and Kado H 1995 Development of a semi-portable DC-SQUID magnetometer *IEEE Trans. Appl. Supercond.* **5** 2474–7
[111] Buckley J R, Khare N, Donaldson G B, Cochran A and Hui Z 1991 Use of a bulk high T_c magnetometer for non-destructive evaluation *IEEE Trans. Magn.* **27** 3051–4
[112] Donaldson G B, Bowman R M, Cochran A, Kirk K J, Pegrum C M and Macfarlane J C 1992 Progress in high T_c magnetic sensors and their applications *Phys. Scr.* T **45** 34–40
[113] Bowman R M, MacFarlane J C, Cochran A, Kirk K J, Pegrum C M and Donaldson G B 1993 Assessment of HTS step-edge thin-film RF SQUIDs for NDT *Supercond. Sci. Technol.* **6** 91–5
[114] Cochran A, Macfarlane J C, Morgan L N C, Kuznik J, Weston R, Hao L, Bowman R M and Donaldson G B 1994 Using a 77 K SQUID to measure magnetic fields for NDE *IEEE Trans. Appl. Supercond.* **4** 128–35
[115] Carr C, Cochran A, Kuznik J, McKirdy D McA and Donaldson G B 1996 Electronic gradiometry for NDE in an unshielded environment with stationary and moving HTS SQUIDs *Cryogenics* **36** 691–6
[116] Klein U, Walker M E, Cochran A, Hutson D, Weston R G and Pegrum C M 1995 Experimental characterisation of planar SQUID gradiometers in niobium technology *Appl. Supercond. 1995* ed D Dew-Hughes (Bristol: IOP) pp 1633–6
[117] Walker M E, Cochran A, Klein U, Bain R J P and Donaldson G B 1995 Modelled response of planar asymmetric gradiometers *Appl. Supercond. 1995* ed D Dew-Hughes (Bristol: IOP) pp 1597–600
[118] Tavrin Y A, Xu Y, Braginski A I, Heiden C, Linnik A S, Pavliuk V A and Schapovalenko V V 1993 Two-hole bulk high T_c SQUID electronic gradiometer for magnetocardiography in unshielded space *Cryogenics* **33** 719–23
[119] Tavrin Y, Zhang Y, Mück M, Braginski A I and Heiden C 1993 $YBa_2Cu_3O_{7-x}$ thin film SQUID gradiometer for biomagnetic measurements *Appl. Phys. Lett.* **62** 1824–6
[120] Tavrin Y, Zhang Y, Wolf W and Braginski A I 1994 A second-order SQUID gradiometer operating at 77 K *Supercond. Sci. Technol.* **7** 265–8
[121] Zhang Y, Tavrin Y, Krause H-J, Bousack H, Braginski A I, Kalberkamp U, Matzander U, Burghoff M and

Trahms L 1995 Applications of high-temperature SQUIDs *Appl. Supercond.* **3** 367
[122] Lucia M L, Hohmann R, Wolf W, Soltner H, Krause H-J, Bousak H, Buschmann H, Spörl G and Binneberg A 1995 Operation of HTS SQUIDs using a cryostat independent of orientation *Dresdener Kolloquium: Kühlsyteme für Elektronische Bauelemente* December 1995
[123] Krause H-J ISI-KFA, Germany. Private communication
[124] Goodman W L and Deaver B S 1970 Detailed measurements of the quantized flux states of hollow superconducting cylinders *Phys. Rev. Lett.* **24** 870–3
[125] Rogers F P 1983 A device for experimental observation of flux vortices trapped in superconducting thin films *Masters Thesis* MIT
[126] Mathai A, Song D, Gim Y and Wellstood F C 1992 One-dimensional magnetic flux microscope based on the dc superconducting quantum interference device *Appl. Phys. Lett.* **61** 598–600
[127] Mathai A, Song D, Gim Y and Wellstood F C 1993 High resolution magnetic microscopy using a dc SQUID *IEEE Trans. Appl. Supercond.* **3** 2609–16
[128] Black R C, Mathai A, Wellstood F C, Dantsker E, Miklich A H, Nemeth D T, Kingston J J and Clarke J 1994 Eddy current microscopy using a 77 K superconducting sensor *Appl. Phys. Lett.* **62** 2128–30
[129] Black R C, Wellstood F C, Dantsker E, Miklich A H, Kingston J J, Nemeth D T and Clarke J 1994 Eddy current microscopy using a 77 K superconducting sensor *Appl. Phys. Lett.* **64** 100–2
[130] Black R C, Wellstood F C, Dantsker E, Miklich A H, Nemeth D T, Koelle D, Ludwig F and Clarke J 1995 Microwave microscopy using a superconducting quantum interference device *Appl. Phys. Lett.* **66** 99–101
[131] Black R C, Wellstood F C, Dantsker E, Miklich A H, Koelle D, Ludwig F and Clarke J 1995 Imaging radio-frequency fields using a scanning SQUID microscope *Appl. Phys. Lett.* **66** 1267–9
[132] Vu L N, Wistrom M S and Van Harlingen D J 1993 Design and implementation of a scanning SQUID microscope *IEEE Trans. Appl. Supercond.* **3** 1918–21
[133] Tsuei C C, Kirtley J R, Chi C C, Yu-Jahnes L S, Gupta A, Shaw T, Sun J Z and Ketchen M B 1994 Pairing symmetry flux quantization in tricrystal superconducting ring of $YBa_2Cu_3O_{7-\delta}$ *Phys. Rev. Lett.* **73** 593–6
[134] Black R C 1995 Magnetic microscopy using a superconducting quantum interference device *PhD Thesis* University of Maryland, 1995
[135] Lee T S, Dantsker E and Clarke J 1996 Scanning high-T_c SQUID system for room-temperature samples *Bull. Am. Phys. Soc.* March Meeting 1996; http://aps.org/BAPSMAR96/
[136] Lee T S University of California at Berkeley. Personal communication
[137] Wikswo J P Jr 1993 Design considerations for magnetic imaging with SQUID microscopes and arrays *Proc. 4th Int. Superconductive Electronics Conf.* pp 189–90
[138] Vrba J *et al* 1993 Whole cortex 64 channel system for shielded and unshielded environments *Proc. 9th Int. Conf. on Biomagnetism* (Amsterdam: Elsevier)
[139] Drung D, Crocoll E, Herwig R, Neuhas M and Jutzi W 1989 Measured performance parameters of gradiometers with digital output *IEEE Trans. Magn.* **25** 1034–7
[140] Brandenburg G, Clements U, Halling H and Zimmermann F 1994 *Internal Report* Zentrallabor für Elektronik, Forschungszentrum Jülich (KFA)
[141] Kung P J, Bracht R R, Flynn E R and Lewis P S 1996 A direct current superconducting quantum interference device gradiometer with a digital signal processor controlled flux-locked loop and comparison with a conventional analog feedback scheme *Rev. Sci. Instrum.* **67** 222–9
[142] Fujimaki N, Tamura H, Suzuki H, Imamura T, Hasuo S and Shibatomi A 1988 A single-chip SQUID magnetometer *IEEE Trans. Electron. Dev.* **35** 2412–7
[143] Radparvar M and Rylov S 1995 An integrated digital SQUID magnetometer with high sensitivity input *IEEE Trans. Appl. Supercond.* **5** 2142–5
[144] Yuh P-F and Rylov S 1995 An experimental digital SQUID with large dynamic range and low noise *IEEE Trans. Appl. Supercond.* **5** 2129–32
[145] Radparvar M Hypres Inc. Personal communication
[146] Wikswo J P Jr 1996 The magnetic inverse problem *NATO ASI Series, SQUID Sensors: Fundamentals, Fabrication and Applications* ed H Weinstock (Berlin: Springer) at press
[147] Rabiner L R and Gold B 1975 For extensive coverage of the theory and practice of DSP *Theory and Application of Digital Signal Processing* (Engelwood Cliffs, NJ: Prentice-Hall)
[148] Press W H, Teukolsky S A, Vetterling W T and Flannery B P 1992 Algorithms for implementation *Numerical Recipes in C* 2nd edn (Cambridge: Cambridge University Press)
[149] Barbosa C H, Bruno A C, Scavarda L F, Lima E A, Ribeiro P C and Kelber C 1995 Image processing technique for NDE SQUID system *IEEE Trans. Appl. Supercond.* **5** 2478–81
[150] Morgan L N C, Carr C, Cochran A, McKirdy D McA and Donaldson G B 1995 Electromagnetic nondestructive evaluation with simple HTS SQUIDs: Measurement and modelling *IEEE Trans. Appl. Supercond.* **5** 3127–30
[151] McKirdy D McA, Cochran A, McNab A and Donaldson G B 1995 Using SQUIDs to solve some current problems in eddy current testing *Appl. Supercond. 1995* ed D Dew-Hughes (Bristol: IOP) pp 1515–18
[152] McKirdy D McA, Cochran A, Donaldson G B and McNab A 1996 Forward and inverse processing in electromagnetic NDE using SQUIDs *Review of Progress in QNDE* vol 15 ed D O Thompson and D Chimenti (New York: Plenum) pp 347–54
[153] Roth B J, Sepulveda N G and Wikswo J P Jr 1989 Using a magnetometer to image a two-dimensional current distribution *J. Appl. Phys.* **65** 361–72
[154] Tan S 1992 Linear system imaging and its application to high-T_c thin films and normal conductors *PhD Dissertation* Department of Physics and Astronomy, Vanderbilt University, Nashville, TN
[155] Tan S, Ma Y P, Thomas I M and Wikswo J P Jr 1993 High resolution SQUID imaging of current and magnetization distributions *IEEE Trans. Appl. Supercond.* **3** 1945–8
[156] Tan S, Sepulveda N and Wikswo J P Jr 1995 A new finite-element approach to reconstruct a bounded and discontinuous two-dimensional current image from a magnetic field map *J. Comp. Phys.* **122** 150–64
[157] Kirtley J R, Ketchen M B, Stawiasz K G, Sun J Z, Gallagher W J, Blanton S H and Wind S J 1995 High resolution scanning SQUID microscope *Appl. Phys. Lett.* **66** 1138–40